

การเติมคูโหละบนไทเทเนี่ยมไดออกไซด์ใช้ในปฏิกิริยาการแยกน้ำด้วยแสง



นาย เอกชัย มานะทิวสน

สถาบันวิทยบริการ

วิทยานิพนธ์นี้เป็นส่วนหนึ่งของการศึกษาตามหลักสูตรปริญญาวิศวกรรมศาสตรมหาบัณฑิต

สาขาวิชาวิศวกรรมเคมี ภาควิชาวิศวกรรมเคมี

คณะวิศวกรรมศาสตร์ จุฬาลงกรณ์มหาวิทยาลัย

ปีการศึกษา 2550

ลิขสิทธิ์ของจุฬาลงกรณ์มหาวิทยาลัย

BIMETALLIC DOPING OF TITANIUM DIOXIDE FOR USE IN  
PHOTOCATALYTIC SPLITTING OF WATER



Mr. Eakachai Manatiwson

สถาบันวิทยบริการ  
จุฬาลงกรณ์มหาวิทยาลัย

A Thesis Submitted in Partial Fulfillment of the Requirements  
for the Degree of Master of Engineering Program in Chemical Engineering

Department of Chemical Engineering

Faculty of Engineering

Chulalongkorn University

Academic Year 2007

Copyright of Chulalongkorn University

Thesis Title            **BIMETALLIC DOPING OF TITANIUM DIOXIDE FOR USE  
IN PHOTOCATALYTIC SPLITTING OF WATER**

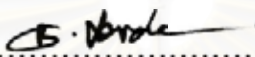
By                         **Mr. Eakachai Manatiwson**

Field of Study         **Chemical Engineering**

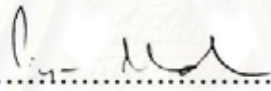
Thesis Advisor        **Akawat Sirisuk, Ph.D.**

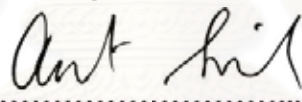
---

Accepted by the Faculty of Engineering, Chulalongkorn University in Partial  
Fulfillment of the Requirements for the Master's Degree

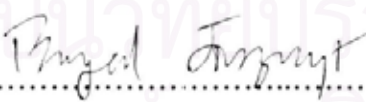
.....Dean of the Faculty of Engineering  
(Associate Professor Boonsom Lerthirunwong, Dr. Ing.)

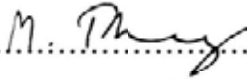
#### THESIS COMMITTEE

.....Chairman  
(Professor Piyasan Prasertdam, Dr. Ing.)

.....Thesis Advisor  
(Akawat Sirisuk, Ph.D.)

.....External Member  
(Assistant Professor Okorn Mekasuwandumrong, Ph.D.)

..... Member  
(Assistant Professor Bunjerd Jongsomjit, Ph.D.)

.....Member  
(Associate Professor Muenduen Phisalaphong, Ph.D.)

เอกชัย มานะทิวสน : การเติมโลหะบนไทเทเนียมไดออกไซด์ใช้ในปฏิกิริยาการแยกน้ำด้วยแสง

(BIMETALLIC DOPING OF TITANIUM DIOXIDE FOR USE IN PHOTOCATALYTIC

SPLITTING OF WATER); อ. ที่ปรึกษา: อ. ดร.อัศวัด ศิริสุข, 64 หน้า

งานวิจัยนี้ศึกษาผลของไทเทเนียมไดออกไซด์โดยทำการเติมโครเมียมไปพร้อมกับแพลทินัมหรือโรเดียมในปริมาณที่เหมาะสมเพื่อเพิ่มประสิทธิภาพปฏิกิริยาการแยกน้ำด้วยแสง ไทเทเนียมไดออกไซด์เตรียมโดยวิธีโซล-เจลและทำการเติมโลหะด้วยวิธีการเคลือบฝังโดยทำการเปลี่ยนแปลงปริมาณโครเมียมในช่วง 0 ถึง 1 % โดยน้ำหนักและทำการเติมโลหะตัวที่สอง (แพลทินัมหรือโรเดียม) ปริมาณ 1 % โดยน้ำหนัก ทำการวิเคราะห์คุณสมบัติของตัวเร่งปฏิกิริยาดังกล่าวด้วยเครื่องมือต่างๆ เช่น ยูวีวิสทิฟิเวอรีแฟกแตนซ์ เอ็กซ์เรย์ดิฟแฟคโตมิเตอร์ การดูดซับในโตรเจนทางกายภาพ กล้องจุลทรรศน์อิเล็กตรอนชนิดส่องผ่าน เอ็กซ์เรย์โฟโตอิเล็กตรอนสเปกโตรสโคปี และโฟโตลูมิเนสเซนซ์ พบว่าการเติมโครเมียมลงไป 0.05 % โดยน้ำหนักเป็นการเพิ่มความว่องไวในปฏิกิริยาการแยกน้ำด้วยแสงเพราะโครเมียมที่เติมลงไปสามารถช่วยลดการกลับมารวมตัวของอิเล็กตรอนกับโฮลในไทเทเนียมไดออกไซด์ อย่างไรก็ตามเมื่อเติมปริมาณโครเมียมไปมากกว่า 0.05 % โดยน้ำหนัก ความว่องไวในปฏิกิริยาการแยกน้ำด้วยแสงจะลดลงเพราะโลหะที่เติมช่วยเพิ่มการกลับมารวมตัวของอิเล็กตรอนกับโฮลในไทเทเนียมไดออกไซด์ จากการวัดด้วยเครื่องโฟโตลูมิเนสเซนซ์พบว่าไทเทเนียมไดออกไซด์ที่มีโครเมียม 0.05 % โดยน้ำหนักให้สัญญาณต่ำที่สุดซึ่งแสดงให้เห็นว่าการกลับมารวมตัวของอิเล็กตรอนกับโฮลได้ช้าที่สุด การเติมโครเมียมไปพร้อมกับแพลทินัมหรือโรเดียมสามารถเพิ่มความว่องไวในปฏิกิริยาการแยกน้ำด้วยแสงโดยจากปฏิกิริยาแสดงให้เห็นว่าความว่องไวในปฏิกิริยาการแยกน้ำด้วยแสงสูงสุดเมื่อทำการเติม 0.01 % โดยน้ำหนักของโครเมียมกับ 1 % โดยน้ำหนักของแพลทินัมหรือโรเดียม ปริมาณโลหะที่เหมาะสมสามารถอธิบายได้ด้วยเหตุผลที่กล่าวมาข้างต้น นอกจากนั้นยังพบการทำงานร่วมกันระหว่างโครเมียมและโลหะตัวที่สองโดยปริมาณก๊าซไฮโดรเจนที่ได้จากปฏิกิริยาการแยกน้ำด้วยแสงด้วยไทเทเนียมไดออกไซด์ที่เติมโครเมียมไปพร้อมกับแพลทินัมหรือโรเดียมจะให้ผลรวมของปริมาณไฮโดรเจนได้มากกว่าปฏิกิริยาบนไทเทเนียมไดออกไซด์เติมโลหะชนิดใดชนิดหนึ่งเพียงชนิดเดียว

สถาบันวิทยบริการ  
จุฬาลงกรณ์มหาวิทยาลัย

ภาควิชา.....วิศวกรรมเคมี..... ลายมือชื่อนิสิต..... ๒๐๕๖..... ๘๖๖๖๖๖๖

สาขาวิชา.....วิศวกรรมเคมี..... ลายมือชื่ออาจารย์ที่ปรึกษา..... 

ปีการศึกษา.....2550.....



##4970715521: MAJOR CHEMICAL ENGINEERING

KEY WORD: TITANIUM DIOXIDE/ PHOTOCATALYTIC WATER SPLITTING  
/BIMETALLIC DOPING.

EAKACHAI MANATIWSON: BIMETALLIC DOPING OF TITANIUM  
DIOXIDE FOR USE IN PHOTOCATALYTIC SPLITTING OF WATER.  
THESIS ADVISOR: AKAWAT SIRISUK, Ph.D, 64 pp.

In this study, titanium dioxide was loaded with chromium together with either platinum or rhodium in attempt to improve its photocatalytic activity for water splitting. Titanium dioxide was synthesized via a sol-gel method and the metals were loaded by incipient wetness impregnation technique. The amount of chromium added was varied between 0 to 1 % (w/w), while the amount of the second metals (either Pt or Rh) added was fixed at 1 % (w/w). The catalysts were characterized by UV-visible diffuse reflectance spectroscopy, X-ray diffraction (XRD), nitrogen physisorption, transmission electron microscopy (TEM), and photoluminescence. Addition of chromium up to 0.05 % (w/w) enhanced the photocatalytic activity because chromium prevented recombination of photogenerated electrons and holes in titanium dioxide. However, when the amount of chromium added exceeded 0.05% (w/w), the photocatalytic activity decreased owing to overtrapping of charge carriers by chromium. Photoluminescence measurement also suggested that titanium dioxide loaded with 0.05 % (w/w) Cr, of which photoluminescence signal was the lowest, had the slowest recombination of charge carriers. Addition of chromium together with platinum or rhodium further increased the photocatalytic activity for water splitting. The catalysts that possessed the highest activity were titanium dioxide that was loaded with 0.01 % (w/w) Cr and 1 % (w/w) Pt or Rh. The optimal loading of the metals could be explained by the similar reason above. Furthermore, a synergy between chromium and the other metal was observed. The amount of hydrogen gas produced from photocatalytic water splitting over titanium dioxide loaded with chromium together with either platinum or rhodium was greater than the sum of the amount of hydrogen gas produced from the reaction over either metal alone.

Department.....Chemical Engineering..... Student's signature... *Eakachai Manatison*  
Field of study....Chemical Engineering..... Advisor's signature... *Akawat Sirisuk*  
Academic year.....2007.....

## ACKNOWLEDGEMENTS

The author would like to express his sincere gratitude and appreciation to his advisor, Dr. Akawat Sirisuk , for his invaluable suggestions, encouragement during his study, useful discussions throughout this research and especially, giving his the opportunity to present his research at PACCON 2008 conference in Thailand. In addition, the author would also be grateful to Professor Piyasan Prasertdam, as the chairman, Assistant Professor Bunjerd Jongsomjit, Assistant Professor Muenduen Phisalaphong, Assistant Professor Okorn Mekasuwandumrong and as the members of the thesis committee. The financial supports of the Thailand Research Fund (TRF) and the Graduate School of Chulalongkorn University are gratefully acknowledged.

Most of all, the author would like to express his highest gratitude to his parents who always pay attention to his all the times for suggestions and listen his complain. The most success of graduation is devoted to my parents.

The author would like to acknowledge with appreciation to Assistant Professor Jungjai for their kind suggestions on his research without hesitation.

Finally, the author wishes to thank the members of the Center of Excellence on Catalysis and Catalytic Reaction Engineering, Department of Chemical Engineering, Faculty of Engineering, Chulalongkorn University for friendship. To the many others, not specifically named, who have provided his with support and encouragement, please be assured that he thinks of you.

## CONTENTS

	<b>Page</b>
ABSTRACT (THAI) .....	iv
ABSTRACT (ENGLISH).....	v
ACKNOWLEDGEMENTS.....	vi
CONTENTS.....	vii
LIST OF TABLES.....	ix
LIST OF FIGURES.....	x
CHAPTER	
I INTRODUCTION.....	1
II LITERATURE REVIEWS.....	3
2.1 Photocatalytic decomposition of water to hydrogen on titanium dioxide.....	3
2.2 Roles of metals on titanium dioxide in photocatalytic reaction.....	4
III THEORY.....	9
3.1 Physical and chemical properties of titanium dioxide.....	9
3.2 Preparation of Titanium dioxide via a sol-gel method.....	11
3.3 Reaction mechanism for hydrogen production from photocatalytic water splitting over titanium dioxide.....	12
3.4 Roles of metal in hydrogen production from photocatalytic water splitting over titanium dioxide.....	14
IV EXPERIMENTAL.....	16
4.1 Chemicals.....	16
4.2 Catalyst Preparation.....	16
4.2.1 Preparation of TiO <sub>2</sub> support.....	16
4.2.2 Deposition of metals.....	17
4.3 Photocatalytic reactor.....	17
4.4 Photocatalytic reaction.....	18
4.5 Catalyst Characterization.....	18
4.5.1 X-ray diffraction analysis (XRD).....	19
4.5.2 Surface area measurement.....	19
4.5.3 UV-visible absorption spectroscopy (UV-Vis).....	19
4.5.4 Photoluminescence spectra (PL).....	20

4.5.5 X-ray photoelectron spectroscopy (XPS).....	20
4.5.6 Inductively-coupled plasma atomic emission spectroscopy (ICP-AES).....	20
4.5.7 Electron spin resonance spectroscopy (ESR).....	21
V RESULTS AND DISCUSSION.....	22
5.1 Properties and photocatalytic activity of titanium dioxide loaded with chromium .....	22
5.1.1 Crystallite phase and size.....	22
5.1.2 Specific surface area.....	22
5.1.3 Metal content.....	23
5.1.4 Light absorption characteristics.....	24
5.1.5 Electron spin resonance spectroscopy.....	25
5.1.6 Photoluminescence measurement.....	27
5.1.7 Transmission electron microscopy (TEM).....	27
5.1.8 X-ray photoelectron spectroscopy (XPS).....	28
5.1.9 Photocatalytic activity.....	32
5.2 Properties and photocatalytic activity of titanium dioxide loaded with chromium and 1 % (w/w) platinum.....	34
5.2.1 Crystallite phase and size.....	34
5.2.2 Specific surface area.....	35
5.2.3 Metal content.....	36
5.2.4 Light absorption characteristics.....	37
5.2.5 Electron spin resonance spectroscopy.....	38
5.2.6 Photoluminescence measurement.....	39
5.2.7 Transmission electron microscopy (TEM).....	40
5.2.8 Photocatalytic activity.....	41
5.3 Properties and photocatalytic activity of titanium dioxide loaded with chromium and 1 % (w/w) rhodium.....	44
5.3.1 Crystallite phase and size.....	44
5.3.2 Specific surface area.....	45
5.3.3 Metal content.....	45
5.3.4 Light absorption characteristics.....	46



	viii
	<b>Page</b>
5.3.5 Electron spin resonance spectroscopy.....	46
5.3.6 Photoluminescence measurement.....	48
5.3.7 Photocatalytic activity.....	49
VI CONCLUSION AND RECOMMENDATIONS.....	52
6.1 Conclusion.....	52
6.2 Recommendations for the future studies.....	52
REFERENCES.....	53
APPENDICES.....	58
APPENDIX A CALCULATION FOR CATALYST PREPARATION.	59
APPENDIX B CALCULATION OF THE CRYSTALLITE SIZE.....	60
APPENDIX C CALIBRATION CURVES.....	62
LIST OF PUBLICATION.....	63
VITA.....	64


  
 สถาบันวิทยบริการ  
 จุฬาลงกรณ์มหาวิทยาลัย

## LIST OF TABLES

Table		Page
3.1	Crystallographic properties of anatase, brookite, and rutile.....	11
4.1	Operating condition of gas chromatograph.....	18
5.1	Crystallite size and specific surface area of titanium dioxide with various amounts of Cr loading.....	24
5.2	Chromium content as measured from ICP-AES, on titanium dioxide loaded with various amount of chromium.....	24
5.3	Peak height per unit surface area, as determined from ESR measurement, for titanium dioxide loaded with various amount of Cr.....	26
5.4	Crystallite size and specific surface area of titanium dioxide with various amounts of Cr and 1.0 % (w/w) Pt loading.....	36
5.5	Chromium and 1 % (w/w) platinum content as measured from ICP-AES, on titanium dioxide loaded with various amount of chromium.....	36
5.6	Peak heights per unit surface area, as determined from ESR measurement, for titanium dioxide loaded with various amount of Cr and 1% (w/w) Pt.....	39
5.7	Crystallite size and specific surface area of titanium dioxide with various amounts of Cr and 1.0 % (w/w) rhodium loading.....	45
5.8	Chromium and 1 % (w/w) rhodium content as measured from ICP-AES, on titanium dioxide loaded with various amount of chromium and 1.0 % (w/w) rhodium.....	46
5.9	Peak heights per unit surface area, as determined from ESR measurement, result of titanium dioxide loaded with various amount of Cr and 1% (w/w) Rh.....	47

## LIST OF FIGURES

<b>Figure</b>		<b>Page</b>
2.1	Simplified diagram of the heterogeneous photocatalytic processes occurring on an illuminated semiconductor particle.....	5
3.1	Crystal structures of titanium dioxide in rutile, and anatase.....	11
3.2	Mechanism of TiO <sub>2</sub> photocatalytic water-splitting for hydrogen production.....	13
3.3	Mechanism of metal-dropped titanium dioxide in photocatalytic water-splitting for hydrogen production.....	15
4.1	Experiment set-up of photochemical reactor.....	18
5.1	XRD patterns of titanium dioxide loaded with various amount of chromium.....	23
5.2	UV-visible absorption characteristics of titanium dioxide loaded with various amount of chromium.....	25
5.3	Peak height ESR results of titanium dioxide loaded with various amount of Cr.....	26
5.4	Photoluminescence emission signals in a range of 380-600 nm for titanium dioxide loaded with various amount of chromium.....	28
5.5	Photoluminescence emission signals in ranges of 380-420 nm for titanium dioxide loaded with various amount of chromium.....	29
5.6	Transmission electron micrograph of pure titanium dioxide (magnification is 80,000).....	30
5.7	Transmission electron micrograph of titanium dioxide loaded with 1 % (w/w) Cr (magnification is 100,000).....	30
5.8	Transmission electron micrograph of titanium dioxide loaded with 1 % (w/w) Cr (magnification is 300,000).....	31
5.9	XPS spectrum of the samples containing only Cr.....	31
5.10	XPS spectrum of TiO <sub>2</sub> that was loaded with 10% (w/w) Cr.....	32
5.11	Amount of hydrogen produced from photocatalytic water splitting over titanium dioxide loaded with various amount of chromium...	34
5.12	XRD patterns of titanium dioxide loaded with various amount of chromium and 1.0 % (w/w) platinum.....	35

<b>Figure</b>		<b>Page</b>
5.13	UV-visible absorption characteristics of titanium dioxide loaded with various amount of chromium and 1 % (w/w) platinum.....	37
5.14	ESR results of titanium dioxide loaded with various amount of Cr and 1% (w/w) Pt.....	38
5.15	Photoluminescence emission signals of titanium dioxide loaded with various amount of chromium and 1 % (w/w) platinum.....	40
5.16	TEM micrographs of titanium dioxide loaded with various amount of chromium and 1.0 % (w/w) platinum.....	41
5.17	Amount of hydrogen produced from photocatalytic water splitting over titanium dioxide loaded with various amount of Cr and 1 % (w/w) Pt.....	43
5.18	Amount of hydrogen produced by pure TiO <sub>2</sub> and various amounts of metals in photocatalytic was compared at time 300 mins.....	43
5.19	XRD patterns of titanium dioxide loaded with various amount of chromium and 1.0 % (w/w) rhodium.....	44
5.20	UV-visible absorption characteristics of titanium dioxide loaded with various amount of chromium and 1 % (w/w) rhodium.....	47
5.21	Peak height ESR result of titanium dioxide loaded with various amount of Cr and 1% (w/w) Rh.....	48
5.22	Photoluminescence emission signals of titanium dioxide loaded with various amount of chromium and 1 % (w/w) rhodium.....	49
5.23	Amount of hydrogen produced from photocatalytic water splitting over titanium dioxide loaded with various amount of Cr and 1 % (w/w) Rh.....	50
5.24	Amount of hydrogen produced by pure TiO <sub>2</sub> and various amounts of metals in photocatalytic was compared at time 300 mins.....	51
B.1	The 101 diffraction peak of titanium dioxide for calculation of the crystallite size.....	61
C.1	The calibration curve of hydrogen.....	62

# CHAPTER I

## INTRODUCTION

Hydrogen is considered as an ideal fuel for the future. Hydrogen fuel can be produced from clean and renewable energy sources and, thus, its life cycle is clean and renewable. Solar and wind are the two major sources of renewable energy and they are also the promising sources for renewable hydrogen production. However, presently, renewable energy contributes only about 5% of the commercial hydrogen production primarily via water electrolysis, while other 95% hydrogen is mainly derived from fossil fuels

Titanium dioxide in photocatalytic water splitting technology has great potential for low-cost, environmentally friendly, solar production of hydrogen to support the future hydrogen economy. Presently, the solar-to-hydrogen energy conversion efficiency is too low for the technology to be economically sound. The main barriers are the rapid recombination of photo-generated electron/hole pairs as well as backward reaction and the poor activation of titanium dioxide by visible light. In response to these deficiencies, many investigators have been conducting research with an emphasis on effective remediation methods. Some investigators studied the effects of addition of sacrificial reagents and carbonate salts to prohibit rapid recombination of electron/hole pairs and backward reactions [Gurunathan et al., 1997; Li et al., 2003; Kida et al., 2004; Wu and Chao, 2004]. Other research focused on the enhancement of photocatalysis by modification of titanium dioxide by means of metal loading, metal ion doping, dye sensitization, composite semiconductor, anion doping, and metal ion implantation. [Ni et al., 2005]

The photo-excited electrons can be transferred from the conduction band of titanium dioxide to metal particles deposited on the surface of titanium dioxide, while the photo-generated holes in the valence band remain on the titanium dioxide. These activities greatly reduce the possibility of electron-hole recombination, resulting in efficient separation of charge carriers and better photocatalytic reactions [John et al., 1983; Bamwenda et al., 1995; Sakthivel et al., 2004] In this work, we synthesized titanium dioxide via a sol-gel method [Geula et al., 1993] and loaded a combination of



two metals, i.e., chromium together with either rhodium or platinum. The catalysts were employed in photocatalytic splitting of water.

The objective of the research is to investigate the doping of TiO<sub>2</sub> using two types of metals for use in photocatalytic splitting of water.

The present study is arranged as follows:

Chapter I is the introduction.

Chapter II presents literature survey of the previous works related to this research.

Chapter III describes the basic information about titania, a sol-gel process, and photocatalytic splitting of water.

Chapter IV describes preparation procedures for the catalyst, characterization techniques employed, and the experimental setup.

Chapter V presents the experimental results and discussion.

Chapter VI includes the overall conclusions of this research and recommendation for future works.

สถาบันวิทยบริการ  
จุฬาลงกรณ์มหาวิทยาลัย

## CHAPTER II

### LITERATURE REVIEWS

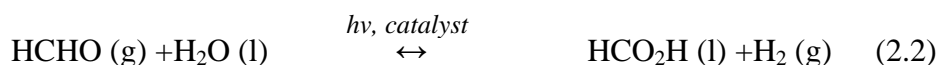
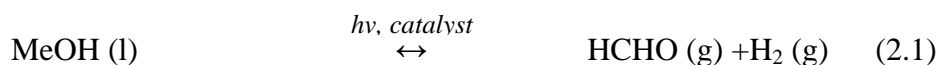
#### 2.1 Photocatalytic decomposition of water to hydrogen on titanium dioxide

Titanium dioxide has drawn tremendous attention for its potential applications in photocatalysis in different fields, because of its high stability and favorable band-gap energy. For hydrogen production from water, many studies have concluded that direct photodecomposition of water into hydrogen and oxygen has a very low efficiency due to rapid reverse reaction. A much higher hydrogen production rate can be obtained by addition of a sacrificial reagent, such as alcohols, carbohydrates solid carbons, sulfide, etc. [Wu and Lee, 2004]. This suggests that photoexcited electrons and holes can be efficiently separated in a small semiconductor particle and that they are available for an irreversible chemical reaction, oxidization of sacrificial reagent. It is, therefore, inferred that a low efficiency of photodecomposition of water into hydrogen and oxygen is mainly due to a rapid reverse reaction between produced hydrogen and oxygen. Thus, a critical problem to be resolved for realizing the up-hill reaction efficiently is how to prevent such thermodynamically favored reverse reaction [Moon et al., 2000].

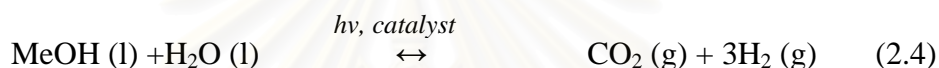
Of particular interest in these intercalated nanoparticles was the production of hydrogen from water containing a sacrificial agent under visible light irradiation with quantum yields as high as 10%. This might be attributable to the ease in donating lone-pair electrons to the valence band hole upon the photocatalyst excitation. Compared to other types of sacrificial reagents among the alcohol series itself, methanol was found to be the most effective and strongest sacrificial reagent to yield the highest photocatalytic H<sub>2</sub> evolution activity.

For hydrogen production from a water/methanol solution, depending on reaction conditions and on whether metal catalyst used, the reaction could proceed

either stepwise, involving stable intermediates, as suggested by Sakata and coworker [1982]:



Or in a one-step reaction on catalyst surface to give the overall reaction, as suggested by Chen and coworkers [1998]:



## 2.2 Roles of metals on titanium dioxide in photocatalytic reaction

The basic principles of heterogeneous photocatalysis can be summarized shortly as follows. A semiconductor is characterized by an electronic band structure in which the highest occupied energy band, called valence band (VB), and the lowest empty band, called conduction band (CB), are separated by a bandgap, i.e., a region of forbidden energies in a perfect crystal. When a photon of energy higher or equal to the bandgap energy is absorbed by a semiconductor particle, an electron from the VB is promoted to the CB with simultaneous generation of a hole ( $h^+$ ) in the VB. The  $e_{cb}^-$  and the  $h_{vb}^+$  can recombine on the surface or in the bulk of the particle in a few nanoseconds (and the energy dissipated as heat) or can be trapped in surface states where they can react with donor (D) or acceptor (A) species adsorbed on or close to the surface of the particle. Thereby, subsequent anodic and cathodic redox reactions can be initiated (see Figure 2.1). Photochemical deposition of noble metals (Pt, Pd, Rh, Ru, Ir, and Os), has been used as an easy technique to improve catalytic and photocatalytic efficiencies. Addition of noble metals to titanium dioxide was found to be beneficial for the photocatalysis. [Litter et al., 1999]

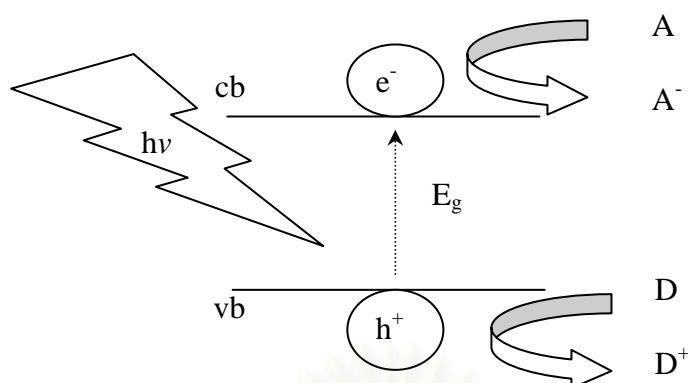


**Figure 2.1** Simplified diagram of the heterogeneous photocatalytic processes occurring on an illuminated semiconductor particle.

Jin and coworkers [2006] studied visible light induced hydrogen generation (>420 nm) over the dye-sensitized M/titanium dioxide (M = Pt, Ru and Rh). The reaction was observed in the presence of electron donors such as triethanolamine, acetonitrile, and triethylamine. The significant enhancement of quantum yield was achieved via noble metal loading and subsequent dye sensitization of M/ titanium dioxide. In the photocatalytic experiment, the catalyst was suspended in 70 ml of DEA–H<sub>2</sub>O mixture by means of a magnetic stirrer. Prior to irradiation, the suspension of the catalyst was dispersed in an ultrasonic bath and argon was bubbled through the reaction mixture for 40 minutes to completely remove oxygen. The dye-sensitized photocatalysts could produced hydrogen from a DEA–H<sub>2</sub>O mixture with high quantum efficiencies and had good stability under visible light irradiation ( $\lambda > 420$  nm) in the presence of electron donors. The H<sub>2</sub> evolution was enhanced with an increase in the metal loading, which may have resulted from the strong adsorption of eosin on the loading metal.

Wu, Lee, and coworkers [2004] studied the physicochemical properties and photocatalytic activities of transition metal-loaded titanium dioxide catalysts. The transition metal was deposited on titanium dioxide via post-hydrothermal synthesis and photo-assisted reduction/impregnation. The structure of titanium dioxide was preserved upon adding Pd, Cr, and Ag into it. The crystallinity was important for the photocatalytic activity of titanium dioxide based catalysts. The function of transition

metal was to increase the electron-hole recombination time, thereby increasing the catalytic activity.

Anpo and Takeuchi [2003] employed electron spin resonance (ESR) signals to investigate electron transfer from titanium dioxide to platinum particles. It was found that  $\text{Ti}^{3+}$  signals increased with irradiation time but the loading of Pt reduced the amount of  $\text{Ti}^{3+}$ . The occurrence of electron transfer from titanium dioxide to Pt particles was indicated by this observation. The noble metal particles accumulated electrons and their Fermi levels shifted closer to the conduction band of titanium dioxide, resulting in more negative energy levels.

Ikuma and Bessho [2006] studied the effects of the deposition method for platinum and the platinum concentration on the hydrogen production rate of platinum-deposited titanium dioxide. Three different deposition methods were used. The formaldehyde method resulted in the highest rate of hydrogen production. The amount of platinum on titanium dioxide had to be optimized to obtain the highest rate of hydrogen production. The platinum particles on the platinum-deposited titanium dioxide prepared by this method were too small or too thin to be observed by transmission electron microscopy.

Nada and coworkers [2005] studied photocatalytic dehydrogenation of liquid methanol, ethanol, 1-propanol, and 2-propanol over platinized anatase and 366 nm UV radiation. Activities and activation energies for carbonyl compound formation were efficiently identical for the four alcohols over 0.5% Pt/TiO<sub>2</sub> prepared by photodeposition. Activation energy of 20 kJ/mol was associated with photoelectron transport through TiO<sub>2</sub> anatase to Pt particles. Methanol was found to be the most efficient electron donor, as indicated by an increase in the amount of hydrogen.

Sreethawong and coworkers [2007] studied the photocatalytic evolution of hydrogen from water over 0.6 wt% Pt-loaded nanocrystalline mesoporous titanium dioxide. The catalyst was prepared by a single-step sol-gel process with a surfactant template. The highly crystalline photocatalyst possessed a mesoporous characteristic with high surface area and narrow monomodal pore size distribution. The influence of the following operational parameters, i.e. sacrificial reagent type, initial solution pH, photocatalyst concentration, initial sacrificial reagent concentration, and irradiation



time, was investigated. The hydrogen evolution was experimentally found to be strongly affected by all of the above parameters. The optimum values of initial solution pH, photocatalyst concentration, and sacrificial reagent concentration as well as the appropriate type of sacrificial reagent were obtained. Methanol was found to be the most efficient sacrificial reagent among several types of sacrificial reagents investigated. Mild acidic pH values in the range of 5-6 were favorable for the reaction. The optimum photocatalyst and initial methanol concentration were found to be 0.91 g/L and 2.25 M.

Zhu and coworkers [2006] studied Cr<sup>3+</sup>-doped anatase titanium dioxide photocatalysts were prepared by the combination of a sol-gel process with a hydrothermal treatment. Due to the excitation of 3d electron of Cr<sup>3+</sup> to the conduction band of Titanium dioxide, Cr-titanium dioxide showed a good ability for absorbing the visible light to degrade an azoic dye, active yellow XRG. Doping of chromium ions effectively improved the photocatalytic activity under both UV light irradiation and visible light irradiation with an optimal doping concentration of 0.15% and 0.2%, respectively. The special distribution of dopants Cr<sup>3+</sup> appeared to have a good effect on enhancing the photocatalytic activity of Cr-titanium dioxide.

Gratian and coworkers [1995] compared the photocatalytic activities for hydrogen generation of Au-titanium dioxide with Pt- titanium dioxide. The metal contents on titanium dioxide that gave the highest hydrogen yield were in the range of 0.3-1 wt % Pt and 1-2 wt % Au. The exposed surface area of gold had only a small influence on the rate of hydrogen generation. On the other hand, the rate of hydrogen production was strongly dependent on the initial pH of the suspension. A value of pH values in the range of 4-7 gave better yields, whereas highly acidic and basic suspensions resulted in a considerable decrease in the hydrogen yield.

Bamwenda and coworkers [1995] compared hydrogen production from water-ethanol solution using Au-loaded titanium dioxide and Pt-loaded titanium dioxide as photocatalysts. Different metal particle deposition methods, such as deposition-precipitation, impregnation and photodeposition were also tested. The loading of Pt worked better than loading of Au. Furthermore, Au loading prepared by photodeposition worked better than deposition-precipitation and impregnation. The

variations might be explained by the better contact with titanium dioxide active sites for photodeposition method. However, Pt-loaded titanium dioxide was found to be less sensitive to the preparation method.

Maeda and coworkers [2006] examined a two-component cocatalyst consisting of Cr and another transition metal in an attempt to improve the photocatalytic activity of  $(\text{Ga}_{1-x}\text{Zn}_x)(\text{N}_{1-x}\text{O}_x)$  for overall water splitting. The best result was obtained from the catalyst containing 1 wt% Rh and 1.5 wt% Cr.

Ekou and coworkers [2006] prepared bimetallic titanium dioxide - supported Rh-Ge and Pt-Ge catalysts by the catalytic reduction method under hydrogen atmosphere, using a parent monometallic catalyst (Rh or Pt) and a germanium salt dissolved in an aqueous medium. Germanium was effectively deposited by the catalytic reduction technique in great interaction with the parent metal (Rh or Pt) supported on titania.

From the literatures reviews, noble metals (Pt, Au, Pd, Rh, Ni, Cu, and Ag) are very effective for enhancement of titanium dioxide photocatalysis. As the Fermi levels of these noble metals are lower than that of titanium dioxide, photo-excited electrons can be transferred from CB to metal particles deposited on the surface of titanium dioxide, while photo-generated VB holes remain on the titanium dioxide. These activities greatly reduce the possibility of electron-hole recombination, resulting in efficient separation and stronger photocatalytic reactions.

สถาบันวิทยบริการ  
จุฬาลงกรณ์มหาวิทยาลัย

## CHAPTER III

### THEORY

#### 3.1 Physical and chemical properties of titanium dioxide

Titanium dioxide may take on any of the following three crystal structures:

Anatase generally exhibits a higher photocatalytic activity than other types of titanium dioxide. The three forms of titanium (IV) oxide have been prepared in laboratories but only rutile, the thermally stable form, has been obtained in the form of transparent large single crystal. The transformation from anatase to rutile is accompanied by the evolution of ca. 12.6 kJ/mol (3.01 kcal/mol), but the rate of transformation is greatly affected by temperature and the presence of other substances, which may either catalyze or inhibit the reaction. The lowest temperature at which transformation from anatase to rutile takes place at a measurable rate is around 700°C, but this is not a transition temperature. The change is not reversible since  $\Delta G$  for the change from anatase to rutile is always negative.

Brookite has been produced by heating amorphous titanium (IV) oxide, which is prepared from an alkyl titanate or sodium titanate, with sodium or potassium hydroxide in an autoclave at 200 to 600 °C for several days. The important commercial forms of titanium (IV) oxide are anatase and rutile, and they can readily be distinguished by X-ray diffractometry.

Rutile, which tends to be more stable at high temperatures and thus is sometimes found in igneous rocks, anatase, which tends to be more stable at lower temperatures (both belonging to the tetragonal crystal system), and brookite, which is usually found only in minerals and has a structure belonging to the orthorhombic crystal system. The titanium dioxide use in industrial products, such as paint, is almost a rutile type. These crystals are substantially pure titanium dioxide but usually amount of impurities, e.g., iron, chromium, or vanadium, which darken them. A summary of the crystallographic properties of the three varieties is given in Table 3.1

**Table 3.1** Crystallographic properties of anatase, brookite, and rutile.

Properties	Anatase	Brookite	Rutile
Crystal structure	Tetragonal	Orthorhombic	Tetragonal
Optical	Uniaxial, negative	Biaxial, positive	Uniaxial, negative
Density, g/cm <sup>3</sup>	3.9	4.0	4.23
Harness, Mohs scale	5 <sup>1/2</sup> – 6	5 <sup>1/2</sup> – 6	7 – 7 <sup>1/2</sup>
Unit cell	D <sub>4h</sub> <sup>19</sup> .4TiO <sub>2</sub>	D <sub>2h</sub> <sup>15</sup> .8TiO <sub>2</sub>	D <sub>4h</sub> <sup>12</sup> .3TiO <sub>2</sub>
Dimension, nm			
a	0.3758	0.9166	0.4584
b		0.5436	
c	0.9514	0.5135	2.953

The three allotropic forms of titanium dioxide have been prepared artificially but only rutile, the thermally stable form, has been obtained in the form of transparent large single crystal. The transformation from anatase to rutile is accompanied by the evolution of ca. 12.6 kJ/mol (3.01 kcal/mol), but the rate of transformation is greatly affected by temperature and by the presence of other substance which may either catalyze or inhibit the reaction. The lowest temperature at which conversion of anatase to rutile takes place at a measurable rate is ca. 700°C, but this is not a transition temperature. The change is not reversible;  $\Delta G$  for the change from anatase to rutile is always negative.

Although anatase and rutile are both tetragonal, they are not isomorphous (see Figure 3.1). The two tetragonal crystal types are more common because they are easy to make. Anatase occurs usually in near-regular octahedral, and rutile forms slender prismatic crystal, which are frequently twinned. Rutile is the thermally stable form and is one of the two most important ores of titanium.

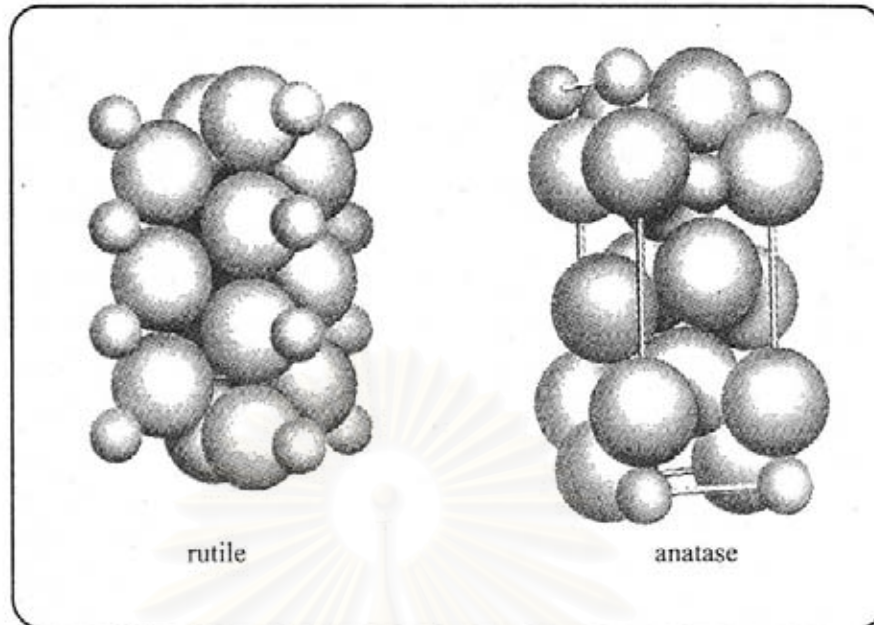
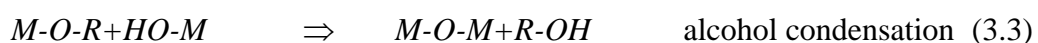
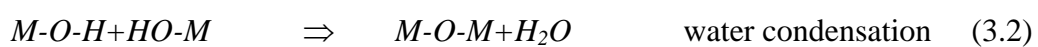
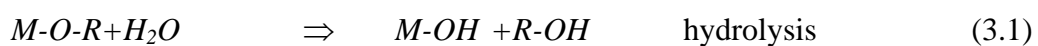


**Figure 3.1** Crystal structures of Titanium dioxide in rutile, and anatase [Fujishima et al., 1999]

Since both anatase and rutile are tetragonal, they are both anisotropic, and their physical properties, e.g. refractive index, vary according to the direction relative to the crystal axes. In most applications of these substances, the distinction between crystallographic directions is lost because of the random orientation of large numbers of small particles, and it is mean value of the property that is significant.

### 3.2 Preparation of Titanium dioxide via a sol-gel method

Sol-gel process occurs in liquid solution of organometallic precursors such as tetraethyl orthosilicate, zirconium propoxide, and titanium isopropoxide, which, by means of hydrolysis and condensation reaction, lead to the formation of sol. [Su. et al., 2004]





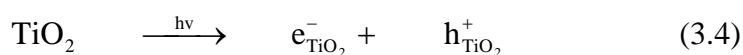
A typical example of a sol-gel method is the addition of metal alkoxides to water. The alkoxides are hydrolyzed, giving the oxide as a colloidal product.

Sol is made of solid particles of a diameter of few hundred nanometers suspending in a liquid phase. After that, the particles condense into gel, in which solid macromolecules are immersed in a liquid phase. Drying the gel at low temperature (25-100 °C) produces porous solid matrices or xerogels. To obtain a final product, the gel is heated. This heat treatment serves several purposes, i.e., to remove solvent, to decompose anions such as alkoxides or carbonates to give oxides, to rearrange of the structure of the solid, and to allow crystallization to occur.

Using a sol-gel method, one can easily control a stoichiometry of solid solution and a homogeneous distribution of nanoparticles and metal oxides. In addition, the metal oxides can be prepared easily at room temperature and high purity can be obtained

### **3.3 Reaction mechanism for hydrogen production from photocatalytic water splitting over titanium dioxide.**

The electronic structure of a semiconductor plays a key role in semiconductor photocatalysis. Unlike a conductor, a semiconductor consists of the valence band (VB) and the conduction band (CB). Energy difference between these two levels is the band gap ( $E_g$ ). Without excitation, both the electrons and holes are in valence band. When semiconductors are excited by photons with energy equal to or higher than their band gap energy, electrons receive energy from the photons and are thus promoted from VB to CB if the energy gain is higher than the band gap energy level. For semiconductor titanium dioxide, the reaction is expressed as:



The photo-generated electrons and holes can recombine in bulk or on surface of the semiconductor within a very short time, releasing energy in the form of heat or photons. Electrons and holes that migrate to the surface of the semiconductor without

recombination can reduce and oxidize the reactants adsorbed by the semiconductor, respectively. The reduction and oxidation reactions are the basic mechanisms of photocatalytic hydrogen production and photocatalytic water/air purification. Both surface adsorption as well as photocatalytic reactions can be enhanced by nano-sized semiconductors since more reactive surface area is available.

For hydrogen production, the CB level should be more negative than hydrogen production level ( $E_{\text{H}_2/\text{H}_2\text{O}}$ ) while the VB should be more positive than water oxidation level ( $E_{\text{O}_2/\text{H}_2\text{O}}$ ) for efficient oxygen production from water by photocatalysis. The photocatalytic hydrogen production by  $\text{TiO}_2$  is shown in Figure 3.2.

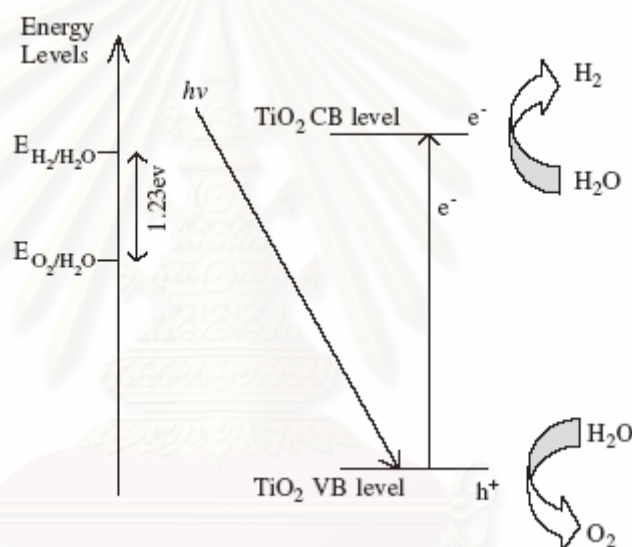


**Figure 3.2** Mechanism of  $\text{TiO}_2$  photocatalytic water-splitting for hydrogen production. [Ni et al., 2005]

Theoretically, all types of semiconductors that satisfy the above-mentioned requirements can be used as photocatalysts for hydrogen production. However, most of the semiconductors that tend to encounter photo corrosion are not suitable for water-splitting. Having strong catalytic activity, high chemical stability and long lifetime of electron/hole pairs, titanium dioxide is the most widely used photocatalyst. Presently, the energy conversion efficiency from solar to hydrogen by photocatalytic water-splitting over titanium dioxide is still low, mainly due to the following reasons:

(1) Recombination of photo-generated electron/hole pairs: CB electrons can recombine with VB holes very quickly and release energy in the form of unproductive heat or photons.

(2) Fast backward reaction: Decomposition of water into hydrogen and oxygen is an energy-increasing process, thus backward reaction (recombination of hydrogen and oxygen into water) easily proceeds.

(3) Inability to utilize visible light: The band gap of titanium dioxide is about 3.2 eV and only UV light can be utilized for hydrogen production. Since the UV light only accounts for about 4% of the solar radiation energy while the visible light contributes about 50%, the inability to utilize visible light limits the efficiency of solar photocatalytic hydrogen production. [Matsuoka et al., 2007]

### 3.4 Roles of metal in hydrogen production from photocatalytic water splitting over titanium dioxide

The addition or impregnation of a transition metal on the TiO<sub>2</sub> photocatalyst surface can enhance the photocatalytic degradation activity by the charge trapping [Brezova et al., 1997; Ikeda et al., 2001; Fuente et al., 2001; Chen et al., 2003; Liqiang et al., 2004; Rajesh et al., 2006; and Zhu et al., 2006]. The charge trapping process is follows that the transfer between metal ions and electron and hole on titanium dioxide can alter electron/hole recombination in equations 3.5 to 3.6.



where M and M<sup>n+</sup> represent metal and the metal ion dopant, respectively.

Here M<sup>n+</sup> was the impregnated metal ion. The energy level of M<sup>n+</sup>/M<sup>(n-1)+</sup> lies below the conduction band edge of TiO<sub>2</sub>. Thus, the energy level of transition metal ions affected the trapping efficiency. The trapping of electrons make it easy for holes to transfer onto the surface of TiO<sub>2</sub> and react with OH<sup>-</sup> in the organic compound solution and form active hydroxyl radicals (OH•), which participate in the degradation of organic compounds. For effective degradation reaction, the recombination of electron and holes was studied. The slow recombination of the holes can be enhanced

by trapping electrons, thereby reducing the recombination of rate and allowing holes to diffuse to the particle surface and participate in oxidation reaction. The electrons in conduction band and protons can combine to form hydrogen [Ni et al., 2005]. If the energy level of dopant ions shifted toward the conduction band edge, the efficiency of trapping becomes higher. In that case, the traps had a larger tendency to act as shallow traps so that the holes generated by following photons cannot recombine with the trapped electrons.

The photocatalytic activity of titanium dioxide loaded with metals for the water splitting resembles other photocatalytic activity. In summary, when  $\text{TiO}_2$  was exposed to UV irradiation, electron migrates from valence band to conduction band of  $\text{TiO}_2$ . The second reduction of surface-adsorbed  $\text{H}^+$  followed by  $\text{H}_2$  formation and oxidation of hole by decomposition of water to oxygen that the addition by impregnation of a transition metal on the titanium dioxide photocatalyst surface can enhance the photocatalytic degradation activity the charge trapping in Figure 3.3.

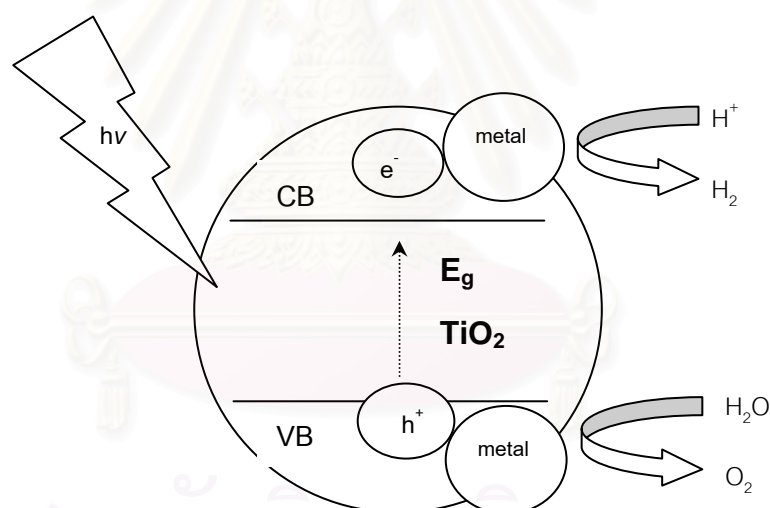


**Figure 3.3** Mechanism of metal-doped titanium dioxide in photocatalytic water-splitting for hydrogen production.

## CHAPTER IV

### EXPERIMENTS

The synthesis of titanium (IV) oxide using a sol-gel method is explained in this chapter. The chemicals, sample preparation and characterization are also explained.

#### 4.1 Chemicals

The details of chemicals used in this research are listed below.

1. Titanium (IV) isopropoxide ( $C_{12}H_{28}O_4Ti$ ) 97%, available from Sigma-Aldrich.
2. Ethanol ( $C_2H_5OH$ ) 99.99%, available from Merck.
3. Nitric acid ( $HNO_3$ ) 70%, available from Asia Pacific Specialty Chemicals Limited.
4. Chromium (III) nitrate nanohydrate ( $Cr(NO_3)_3 \cdot 9H_2O$ ) 99.99%, available from Sigma-Aldrich.
5. Chloroplatinic acid hexahydrate ( $H_2PtCl_6 \cdot 6H_2O$ ) 37.50% Pt, available from Sigma-Aldrich.
6. Sodium hexachlororhodate (III) ( $Na_3RhCl_6$ ) 23.07% Rh, available from Sigma-Aldrich.

#### 4.2 Catalyst Preparation

##### 4.2.1 Preparation of $TiO_2$ support

Titanium dioxide was prepared by the acid-catalyzed sol-gel method. First, the sol was prepared by mixing titanium isopropoxide with ethanol, water, and nitric acid at room temperature while being stirred. For 1 mL of titanium isopropoxide, 20 mL of methanol, 2.3 mL of water, and 0.08 mL of nitric acid were used. To remove solvents, the dialyzed sol was left in ambient atmosphere overnight. Then titanium dioxide gel



was dried at 110 °C for 24 hours [Geula and Micha, 1993]. The resulting gel was ground. Finally, titania was calcined at 350 °C for two hours.

#### 4.2.2 Deposition of metals

Incipient wetness impregnation method was used to deposit chromium, platinum and rhodium. Chromium (III) nitrate nanohydrate ( $\text{Cr}(\text{NO}_3)_3 \cdot 9\text{H}_2\text{O}$ ), Chloroplatinic acid hexahydrate ( $\text{H}_2\text{PtCl}_6 \cdot 6\text{H}_2\text{O}$ ), and Sodium hexachlororhodate (III) ( $\text{Na}_3\text{RhCl}_6$ ) were used as precursors.

To deposit chromium, a desired amount of  $\text{Cr}(\text{NO}_3)_3 \cdot 9\text{H}_2\text{O}$  was dissolved in deionized water, of which volume equaling to the pore volume of the catalyst. The aqueous solution of chromium was added dropwise to the titanium dioxide support. The impregnated support was left at room temperature for six hours to assure adequate distribution of metal complex. After that, the catalyst was dried in the oven at 110 °C overnight. The catalyst was calcined under air flow at the rate of 6 mL/min at 300 °C for two hours.

To deposit chromium together with either platinum or rhodium, desired amounts of the precursors for the two methods were dissolved in deionized water, of which volume equaling to the pore volume of the metal precursors catalyst. The aqueous solution of were added dropwise to the titanium dioxide support. The impregnated support was left at room temperature for six hours to assure adequate distribution of metal complexes. After that, the catalyst was dried in the oven at 110 °C overnight. The catalyst was calcined under air flow at the rate of 6 mL/min at 300 °C for two hours.

#### 4.3 Photocatalytic reactor

Figure 4.1 shows a schematic diagram of a photocatalytic reactor used in this study. The vertical tubular batch reactor was made of Pyrex and has a volume of 125 ml. The reactor was 4 cm in diameter and 24 cm long. Two tubes were placed inside the reactor was connected to argon cylinder and was used to feed argon carrier gas. The other was used vent argon carrier gas.

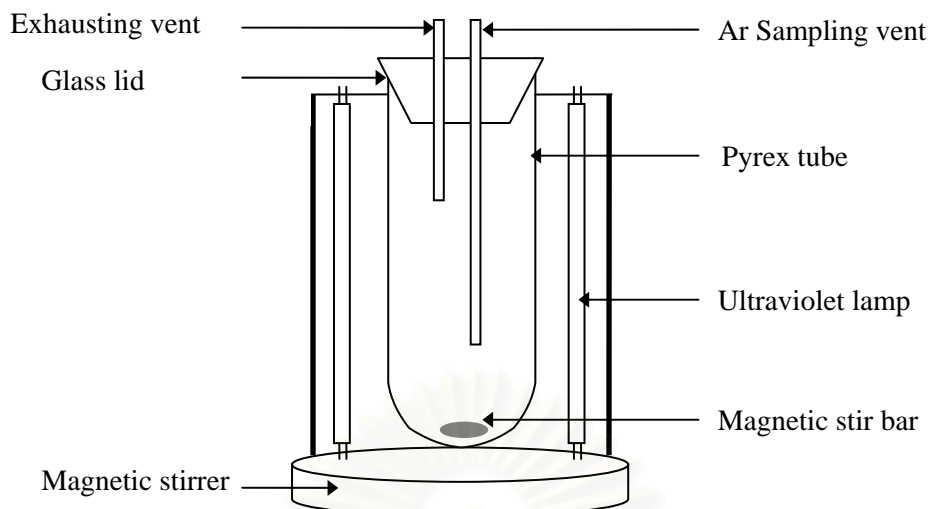


**Figure 4.1** Experiment set-up of photochemical reactor.

Titanium dioxide photocatalyst was suspended by means of a magnetic stirrer and irradiated with eight UV light bulbs (Philips actinic blue), each having a power of 20 W.

**Table 4.1** Operating condition for the gas chromatograph

Gas Chromatograph	SHIMADZU GC-8A
Detector	TCD
Column	Molecular sieve 5A
- Column material	SUS
- Length	2 m
- Outer diameter	4 mm
- Inner diameter	3 mm
- Mesh range	60/80
- Maximum temperature	350 °C
Carrier gas	Ar (99.999%)
Carrier gas flow (ml/min)	30
Initial column temperature (°C)	60
Final column temperature (°C)	60
Injector temperature (°C)	100
Detector temperature (°C)	100
Current (mA)	70
Analyzed gas	Hydrogen

#### 4.4 Photocatalytic reaction

The photocatalytic activity was performed over 0.3 g of titanium dioxide catalyst was suspended in 50 ml of water/methanol solution in the vertical tubular batch reactor. The volume ratio of water to methanol was 4:1. Ultra high purity argon was used to purge the reactor for 120 minutes to remove oxygen inside the reactor. The amount to hydrogen released was determined by a Shimazu GC-8A gas chromatograph equipped with a thermal conductivity detector. The operating conditions for the gas chromatograph are displayed in Table 4.1.

#### 4.5 Catalyst Characterization

The catalysts were characterized by various techniques

##### 4.5.1 X-ray diffraction analysis (XRD)

The XRD spectra were measured by using a SIEMENS D5000 X-ray diffractometer using Cu  $K_{\alpha}$  radiation with a Ni filter. The crystallite size of titanium dioxide was determined from the width at half-height of the (101) diffraction peak of anatase using the Scherrer equation. The condition of the measurement was performed over the  $2\theta$  range of  $20^{\circ}$  to  $80^{\circ}$  and the resolution was  $0.02^{\circ}$ . A total of 10 scans were performed for each sample.

##### 4.5.2 Surface area measurement

The specific surface area of titanium dioxide was measured according to the single point BET method, by using nitrogen as the adsorbate. The weight of the sample was 0.2 g. And the sample was degassed at  $200^{\circ}\text{C}$  prior to the measurement.

##### 4.5.3 UV-visible absorption spectroscopy (UV- Vis)

To study the light absorption behavior of the catalysts, the absorbance spectra of the catalysts in the wavelength range of 200-800 nm were obtained using a Perkin

Elmer Lambda 650 spectrophotometer. The step size for the scan was 1 nm. BaSO<sub>4</sub> was used as a blank for the measurement.

#### 4.5.4 *Photoluminescence spectroscopy (PL)*

Photoluminescence spectra were obtained using a JASCO FP-6200 Spectrofluorometer at room temperature. The amount of sample was used 0.5 g. The sample was mixed with 10 ml of ethanol and was sonicated for two hours. The excitation wavelength was 350 nm with an excitation bandwidth of 5 nm and an emission bandwidth of 10 nm. The measurement was performed over the range of wavelength between 200 and 800 nm with a step size of 1 nm.

#### 4.5.5 *X-ray photoelectron spectroscopy (XPS)*

The XPS analysis was performed using an AMICUS photoelectron spectrometer equipped with a Mg K<sub>α</sub> X-ray as a primary excitation and a KRATOS VISION2 software. XPS elemental spectra were acquired with 0.1 eV energy step at a pass energy of 75 eV. The C<sub>1s</sub> line was taken as an internal standard at 285.0 eV. Photoemission peak areas were determined after smoothing and background subtraction using a linear routine. Deconvolution of complex spectra were done by fitting with Gaussian (70%)-Lorentzian (30%) shapes using a VISION 2 software that came with the XPS system.

#### 4.5.6 *Inductively-coupled plasma atomic emission spectroscopy (ICP-AES)*

Chromium and platinum contents were measured using a Perkin Elmer Optical Emission Spectrometer Optima 2100 DV. To digest the sample, the catalyst was dissolved in 10 ml of 50% HF solution. The mixture was heated to 50 °C and stirred for two hours. After the catalyst was completely digested, the solution was diluted to a volume of 100 ml.

#### 4.5.7 *Electron spin resonance spectroscopy (ESR)*

ESR measurements were carried out using a JEOL JES-RE2X electron spin resonance spectrometer to determine the amount of  $\text{Ti}^{3+}$  surface defect in  $\text{TiO}_2$ . Recorded spectra were scanned and were converted to a g-value scale referring to  $\text{Mn}^{2+}$  marker.



สถาบันวิทยบริการ  
จุฬาลงกรณ์มหาวิทยาลัย



## CHAPTER V

### RESULTS AND DISCUSSION

The results in this chapter are divided into three sections. Section 5.1 describes the properties and photocatalytic activities of titanium dioxide loaded with chromium. Section 5.2 describes the properties and photocatalytic activity of titanium dioxide loaded with chromium and platinum. Finally, Section 5.3 describes properties and photocatalytic activity of titanium dioxide loaded with chromium and rhodium.

#### **5.1 Properties and photocatalytic activity of titanium dioxide loaded with chromium.**

##### *5.1.1 Crystallite phase and size*

The phase identification of titanium dioxide was based on the results from X-ray diffraction analysis (XRD). The XRD patterns of various titanium dioxide loaded with chromium samples were displayed in Figure 5.1. The diffraction peaks at  $2\theta$  values of  $26^\circ$ ,  $37^\circ$ ,  $48^\circ$ ,  $55^\circ$ ,  $56^\circ$ ,  $62^\circ$ ,  $69^\circ$ ,  $71^\circ$ , and  $75^\circ$  indicated that titanium dioxide was primarily in the anatase phase [Suriye et al., 2007]. Small amounts of brookite and rutile were detected in some samples. The average crystallite size of titanium dioxide was estimated from the line broadening of (101) diffraction peak using the Scherrer's equation. The average crystallite size of pure titanium dioxide was approximately 6.2 nm. The crystallite size grew slightly upon the loading of chromium, probably due to the calcination performed after metal deposition.

##### *5.1.2 Specific surface area*

Specific surface areas of the catalysts were determined from nitrogen adsorption isotherms and were displayed in Table 5.1. Pure titanium dioxide possessed the largest specific surface area. Upon addition of chromium, specific surface area decreased. However, the amount of chromium loading appeared to have no significant effects on specific surface area of the catalyst.

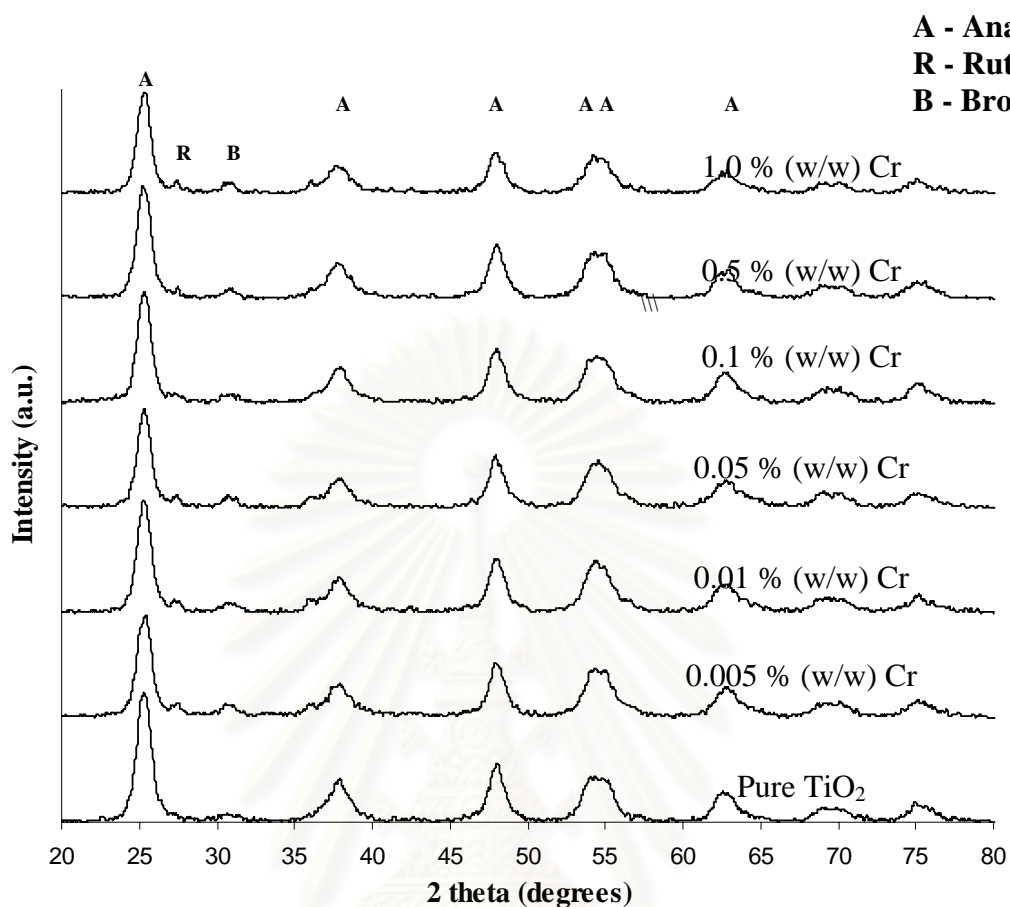


**Figure 5.1** XRD patterns of titanium dioxide loaded with various amount of chromium.

### 5.1.3 Metal content

Percentage of chromium on titanium dioxide catalysts was determined by Inductively couple plasma atomic emission spectroscopy (ICP-AES). The chromium contents in various catalyst samples were listed in Table 5.2. As seen in Table 5.2, the chromium content determined that was ICP-AES was lower than the expected chromium content that was calculated for use during the impregnation step. This discrepancy could be a result of incomplete digestion of ICP-AES sample and uneven distribution of metal on titanium dioxide.

**Table 5.1** Crystallite size and specific surface area of titanium dioxide with various amounts of Cr loading.

<b>Cr loading (% (w/w))</b>	<b>Crystallite size (nm)</b>	<b>Surface area (m<sup>2</sup>/g)</b>
Pure TiO <sub>2</sub>	6.2	141.1
0.005	7.7	88.1
0.01	7.9	94.6
0.05	8.2	100.4
0.1	7.6	98.0
0.5	8.1	92.6
1.0	8.4	100.6

**Table 5.2** Chromium content as measured from ICP-AES, on titanium dioxide loaded with various amount of chromium.

<b>Calculated Cr loading (% (w/w))</b>	<b>Measured Cr content (% (w/w))</b>
0% (w/w) Cr	0
0.005% (w/w) Cr	0.002
0.01% (w/w) Cr	0.004
0.05% (w/w) Cr	0.019
0.1% (w/w) Cr	0.086
0.5% (w/w) Cr	0.215
1.0% (w/w) Cr	0.579

#### 5.1.4 Light absorption characteristics

UV–visible light absorption characteristics of various titanium dioxide loaded with chromium were presented in Figure 5.2. A steep drop in the absorbance at a wavelength longer than 387 nm was assigned to the intrinsic band gap absorption of anatase titanium dioxide (3.2 eV). Addition of chromium extended the absorption band of titanium dioxide to the visible region, while leaving the intrinsic band gap of anatase titanium dioxide unaffected. For titanium dioxide, the light absorption in the visible region provided a possibility for enhancing the photocatalytic activity of TiO<sub>2</sub>.

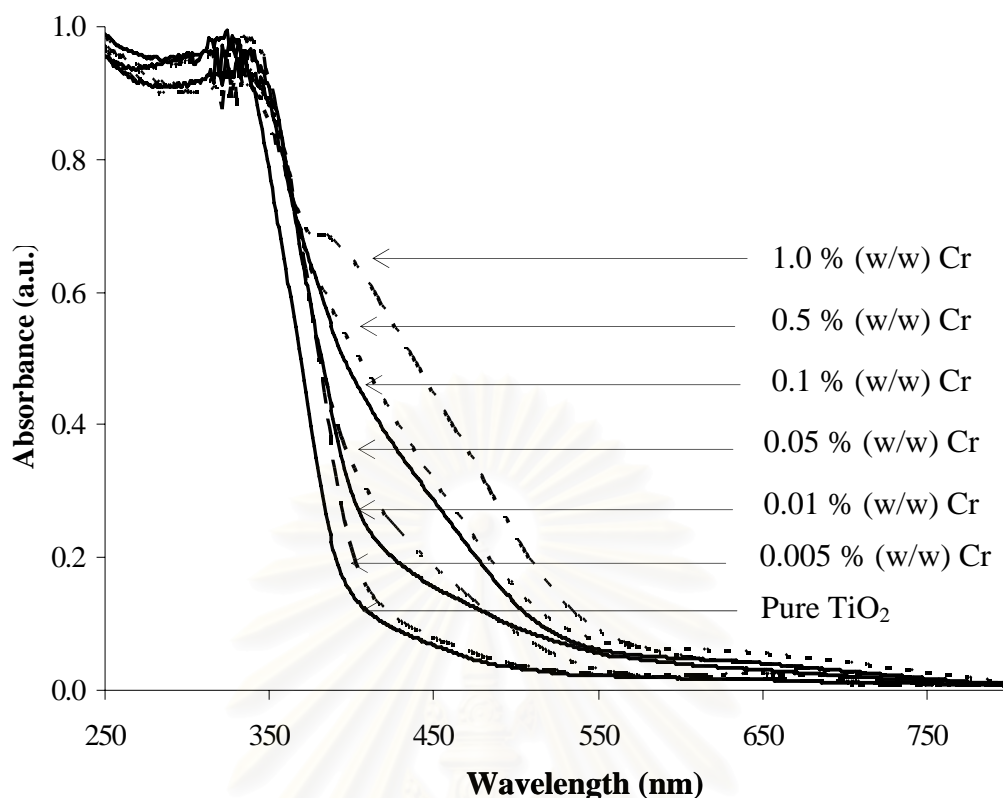


**Figure 5.2** UV-visible absorption characteristics of titanium dioxide loaded with various amount of chromium.

The addition of chromium gave rise to a new absorption shoulder appears at around 420 to 550 nm due to the formation of the impurity energy level within the bandgap of titanium dioxide. As seen in Figure 5.2, an increase in Cr content brought about a better absorption in the visible region for TiO<sub>2</sub> [Anpo and Takeushi, 2003].

#### 5.1.5 Electron spin resonance spectroscopy

Electron spin resonance spectroscopy (ESR) was performed to determine the amount of Ti<sup>3+</sup> defects in the catalyst. Typical result was displayed in Figure 5.3. The peak observed at the g value of 1.97 was assigned to Ti<sup>3+</sup> defects. The peak height was proportional to the amount of Ti<sup>3+</sup> in the catalyst. Table 5.3 listed the peak height per unit surface area of various titanium dioxide samples that were loaded with chromium. From Table 5.3, the amount of Ti<sup>3+</sup> (or the peak height) increased when the chromium content was raised. The higher amount of Cr loading may damage the surface of TiO<sub>2</sub> and from more Ti<sup>3+</sup>.

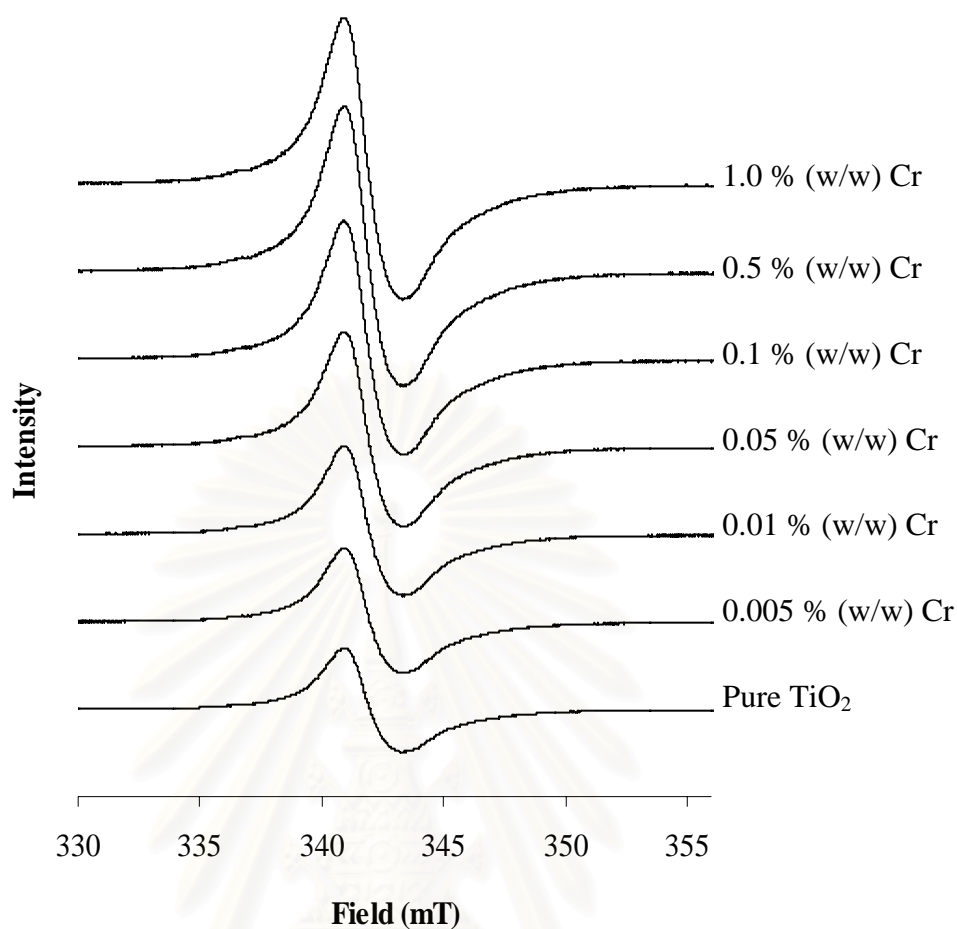


**Figure 5.3** Peak height ESR results of titanium dioxide loaded with various amount of Cr.

**Table 5.3** Peak height per unit surface area, as determined from ESR measurement, for titanium dioxide loaded with various amount of Cr.

Cr loading (% (w/w))	Peak height per unit surface area (1/m <sup>2</sup> )
Pure TiO <sub>2</sub>	70.13
0.005	92.65
0.01	139.71
0.05	250.22
0.1	357.43
0.5	677.94
1.0	679.28



### 5.1.6 Photoluminescence measurement

Photoluminescence emission spectrum was used to investigate the efficiency of charge carrier trapping, immigration, and transfer; and to understand the fate of electrons and holes in titanium dioxide since photoluminescence emission resulted from the recombination of free carriers. Figures 5.4 and 5.5 displayed the photoluminescence spectra for the catalysts that were excited by irradiation with a wavelength of 350 nm at room temperature. Two main emission peaks were observed at wavelengths of 402 and 458 nm, which corresponded to band gap energies of 3.1 and 2.7 eV, respectively. The first emission peak was ascribed to the emission of band gap transition (or the recombination of photogenerated electrons and holes) at a wavelength of 402 nm. The second emission peak was ascribed to the emission signal originated from the energy levels of defects in the band gap, such as oxygen vacancies formed during sample preparation at a wavelength of 458 nm. The oxygen vacancies were generated because of partially incomplete crystallization [Zhao et al., 2007]. The variation in photoluminescence emission spectrum intensity resulted from the change of defect state on the shallow level of the titanium dioxide surface [Zhao and Yu, 2006]. Figure 5.5 revealed that the photoluminescence signal of pure titanium dioxide was the highest among all the samples. Upon addition of chromium (from 0.005 % (w/w) to 0.05% (w/w)), photoluminescence signals were decreased. When the chromium content exceeded 0.05 % (w/w), the photoluminescence signals increased back up again. It can be noticed that 0.05 % (w/w) chromium loaded on titanium dioxide shows the lowest photoluminescence signal.

### 5.1.7 Transmission electron microscopy (TEM)

Transmission electron micrographs of pure  $\text{TiO}_2$  and  $\text{TiO}_2$  loaded with 1 % (w/w) Cr were shown in Figures 5.6 to 5.8, respectively. TEM were performed in order to physically measure the size of the chromium clusters. However, the chromium clusters were not observed because of low chromium loading (less than 1 % (w/w)). Furthermore, the average particle size of  $\text{TiO}_2$  was obtained from the TEM images of the both samples. The average crystallite sizes of pure  $\text{TiO}_2$  and  $\text{TiO}_2$  loaded with 1 % (w/w) Cr were 6.2 nm and 8.1 nm, respectively.

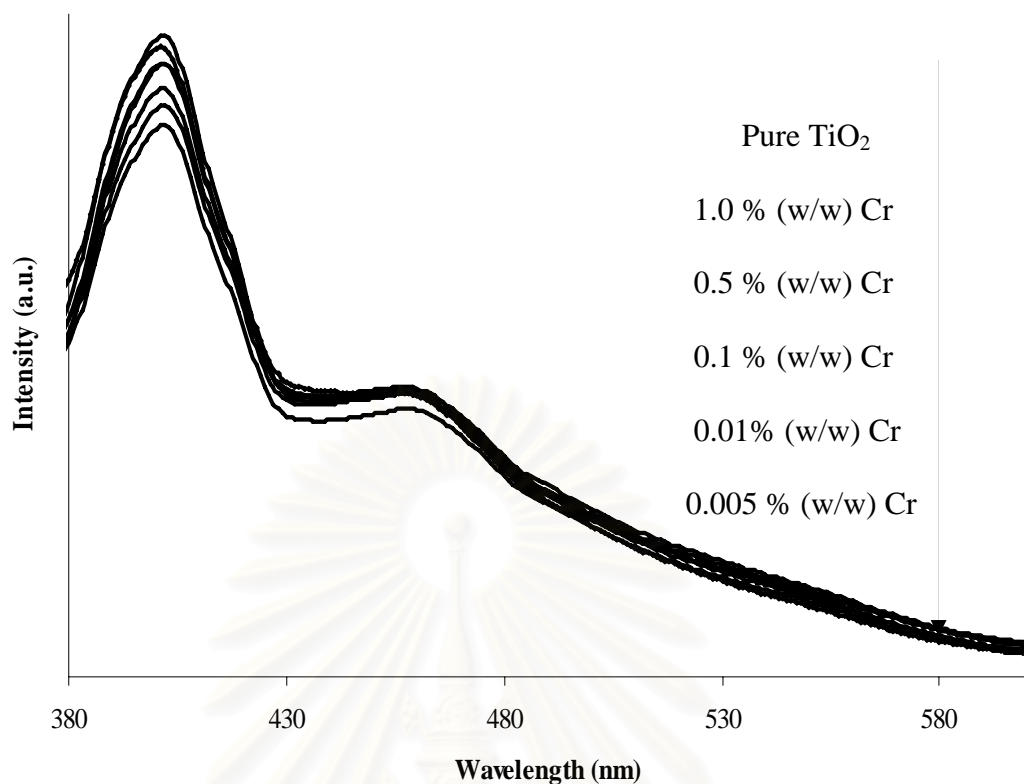


**Figure 5.4** Photoluminescence emission signals in a range of 380-600 nm for titanium dioxide loaded with various amount of chromium.

These results were in good agreement with the average crystallite sizes that were determined from XRD analysis (see Table 5.1)

#### 5.1.8 X-ray photoelectron spectroscopy (XPS)

The XPS spectra for Cr/TiO<sub>2</sub> samples were recorded with a photon energy of 1256 eV (Mg K<sub>α</sub>). For all measurements, the kinetic energies of the emitted electrons in the range of 0-1000 eV were detected. XPS results were obtained for two samples. The first sample contained only Cr, not Ti and was prepared by calcining chromium (III) nitrate nanohydrate at 350 °C for two hours (see Figure 5.9). The second sample was titanium dioxide that was loaded with 10 % (w/w) Cr (see Figure 5.10). The high amount of chromium added was to enhance the signal for chromium in the measurement. From Figures 5.9 and 5.10, the peaks corresponding to chromium 2p were detected at 579.0 eV. This observation suggested the state of chromium in the both samples was Cr<sup>4+</sup>, rather than Cr<sup>3+</sup> (which had a binding energy of 576.6 eV) [Zhu et al., 2006; Nagaveni et al., 2006].

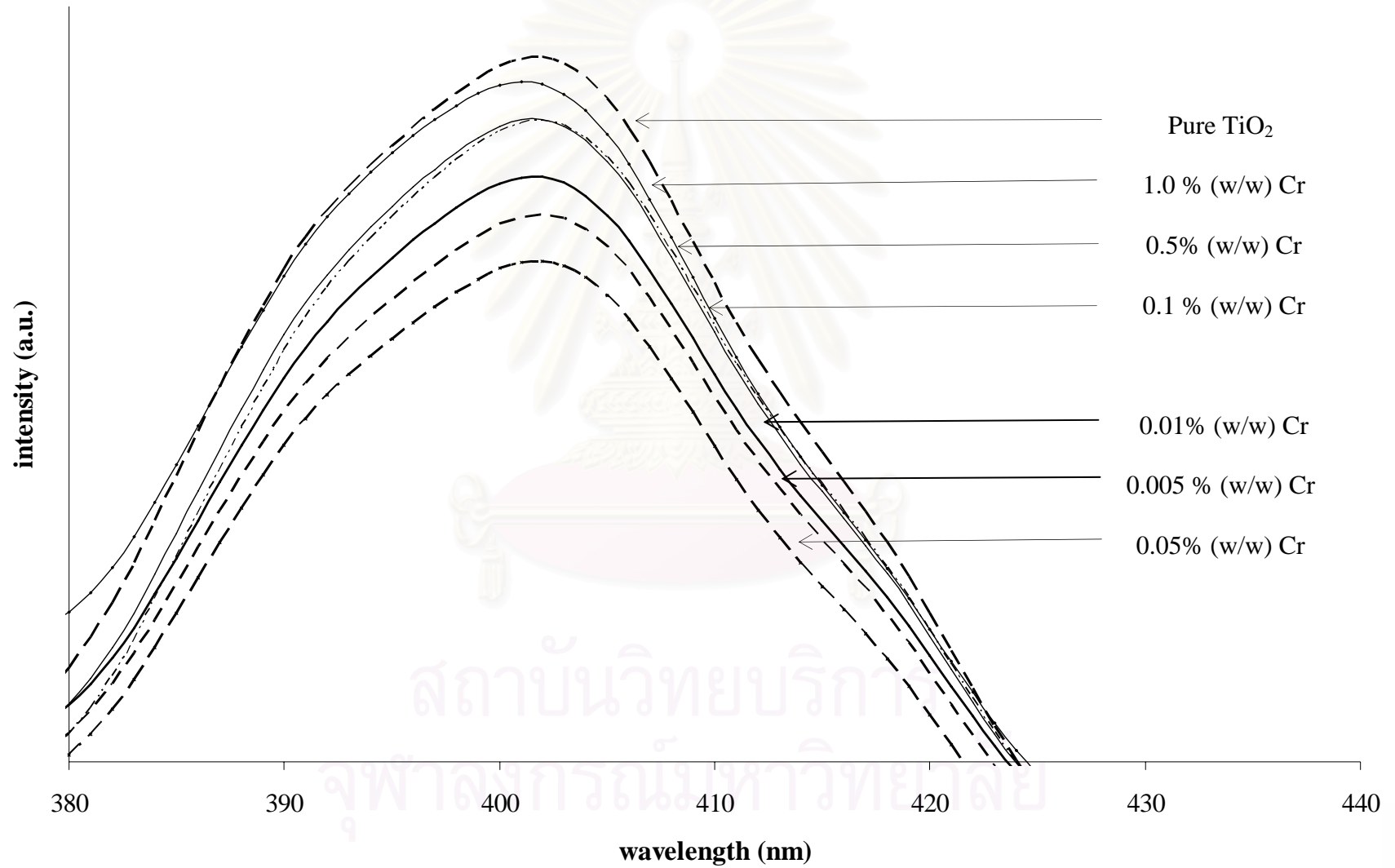


**Figure 5.5** Photoluminescence emission signals in ranges of 380-420 nm for titanium dioxide loaded with various amount of chromium.

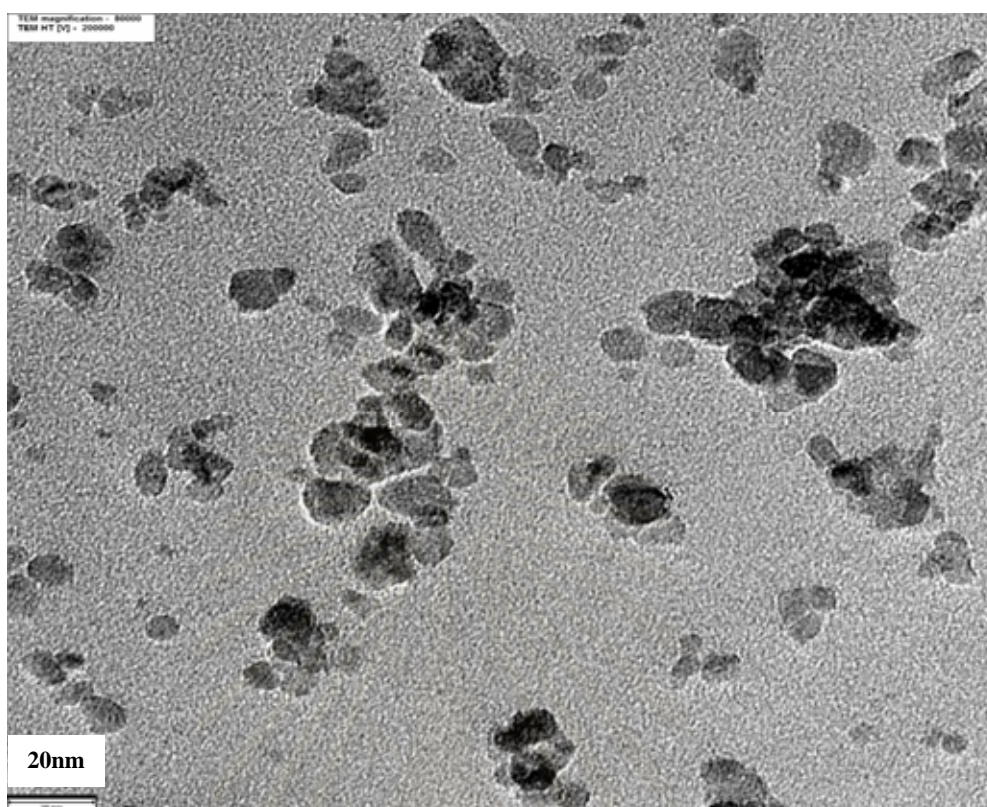


**Figure 5.6** Transmission electron micrograph of pure titanium dioxide (magnification is 80,000).

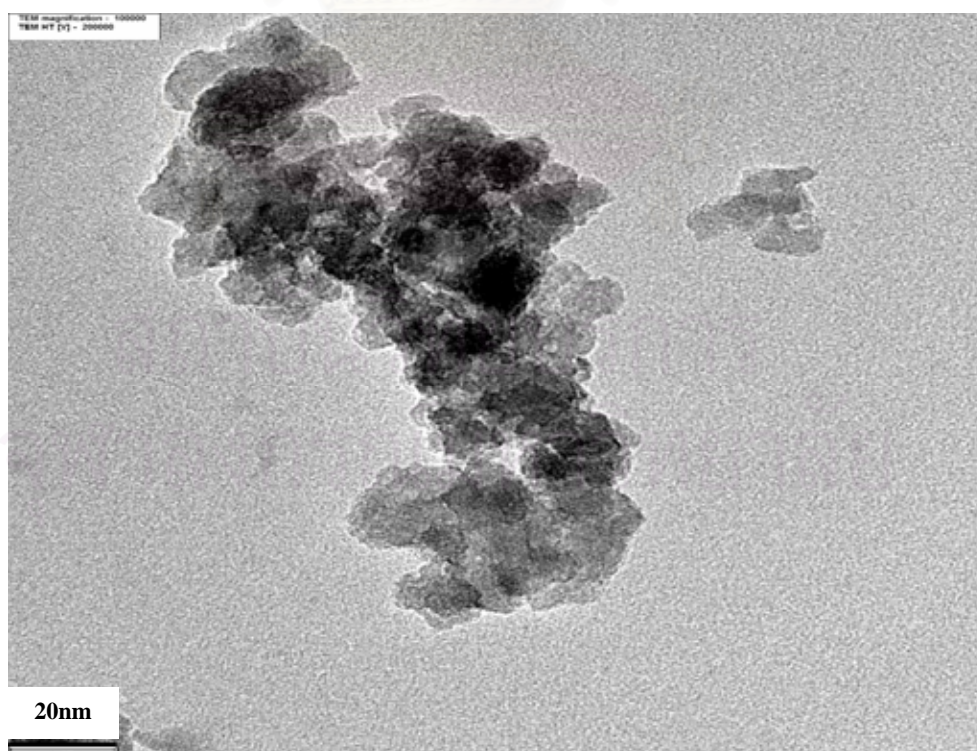


**Figure 5.7** Transmission electron micrograph of titanium dioxide loaded with 1 % (w/w) Cr (magnification is 100,000).



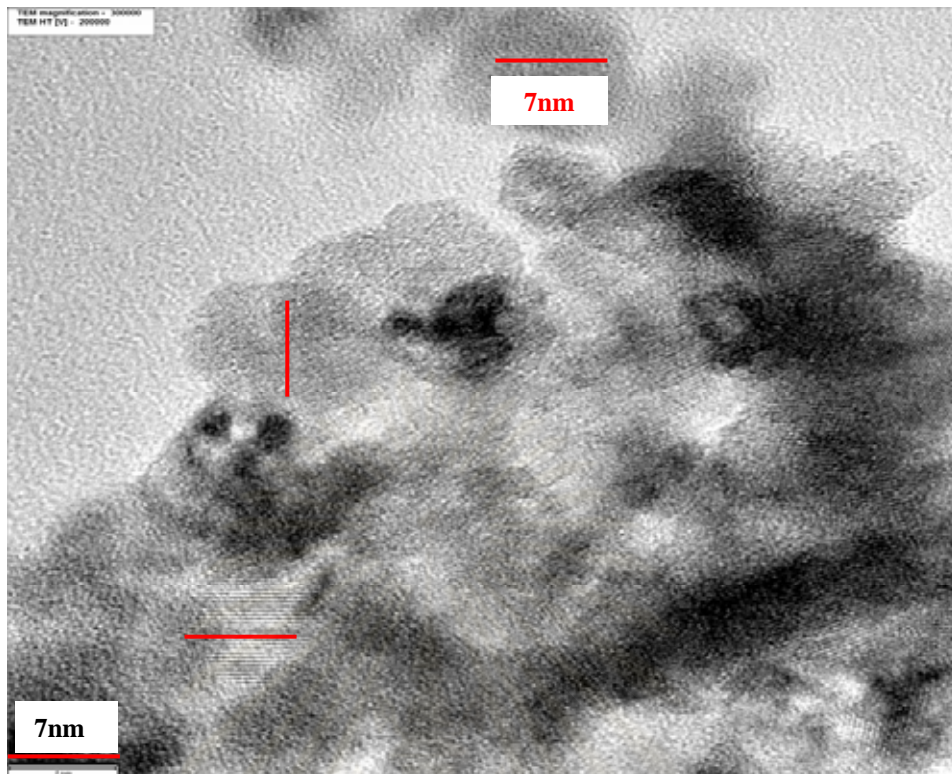


**Figure 5.8** Transmission electron micrograph of titanium dioxide loaded with 1 % (w/w) Cr (magnification is 300,000).

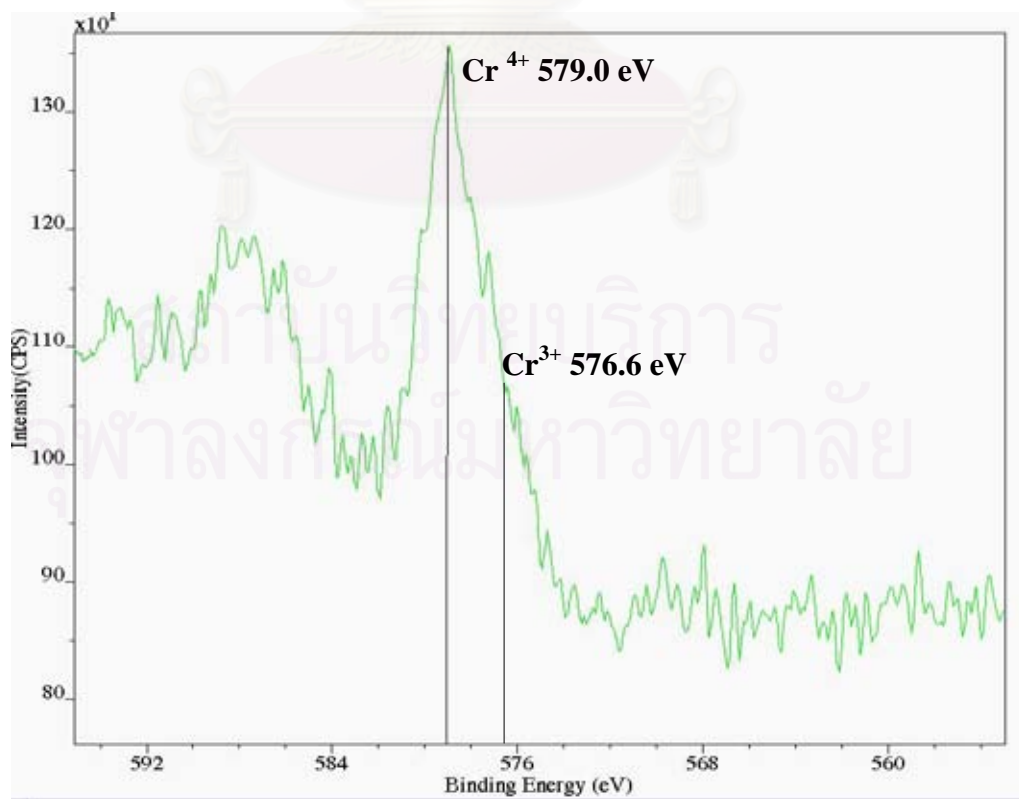


**Figure 5.9** XPS spectrum of the samples containing only Cr.



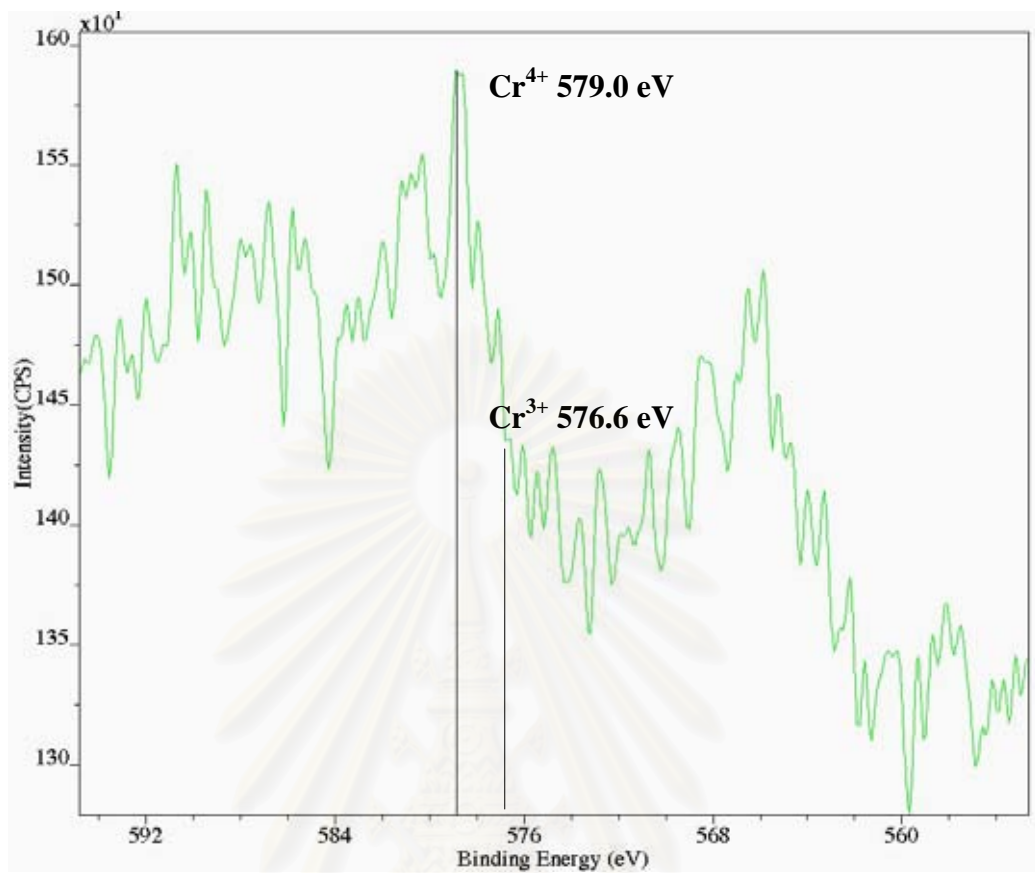


**Figure 5.10** XPS spectrum of TiO<sub>2</sub> that was loaded with 10% (w/w) Cr

### 5.1.9 Photocatalytic activity

Zhu and coworkers, [2006] proposed a reaction mechanism for photocatalytic degradation of organic pollutants over titanium dioxide loaded with chromium. The overall reaction scheme for photocatalytic water splitting was presented in Equations 5.1 to 5.3.



The role of chromium was described by Equations 5.4 to 5.6. Cr<sup>3+</sup> acted as a trap for photogenerated holes (Equation 5.4) because the energy level for Cr<sup>3+</sup>/Cr<sup>4+</sup> lied above the valence band edge of titanium dioxide. The trapped holes in Cr<sup>4+</sup> migrated to the hydroxyl ion adsorbed on TiO<sub>2</sub> surface to produce hydroxyl radicals

(Equations 5.5). The reaction of photogenerated holes with  $\text{Cr}^{3+}$  promoted the separation of photogenerated holes and electrons and improved the photocatalytic activity. Nonetheless  $\text{Cr}^{4+}$ , or trapped holes, could also react with photogenerated electrons (Equations 5.6). In this case,  $\text{Cr}^{3+}$  acted as a recombination center for holes and electrons and was adverse to photocatalytic activity of titanium dioxide.



The photocatalytic activities of titanium dioxide loaded with chromium were quantified by the amount of hydrogen gas produced from the photoreactor. From Figure 5.11, titanium dioxide loaded with 0.05 % (w/w) possessed the highest activity. This result agreed with the result from photoluminescence measurement. The order of decreasing activity (0.05 % (w/w), 0.005 % (w/w), 0.01 % (w/w), and pure titanium dioxide) was the same as the order of increasing photoluminescence signals (see Figure 5.4 and 5.5). The photocatalytic reaction depended on the efficient separation of photogenerated charge carriers in titanium dioxide. Therefore, slower recombination of electrons and holes led to higher photocatalytic activity. As a result, the catalyst with the highest activity should produce the smallest signal in photoluminescence measurement. This agreement was also observed in our case.

Our results were also in good agreement with the results of Zhu and coworkers [2006]. When a small amount of chromium (<0.01 % (w/w)) was added to titanium dioxide. Chromium enhanced the photocatalytic activity by promoting the separation of photogenerated electrons and holes. But when the amount of chromium added was too high, adverse effect on the photocatalytic activity was observed because chromium becomes a recombination center for electrons and holes.

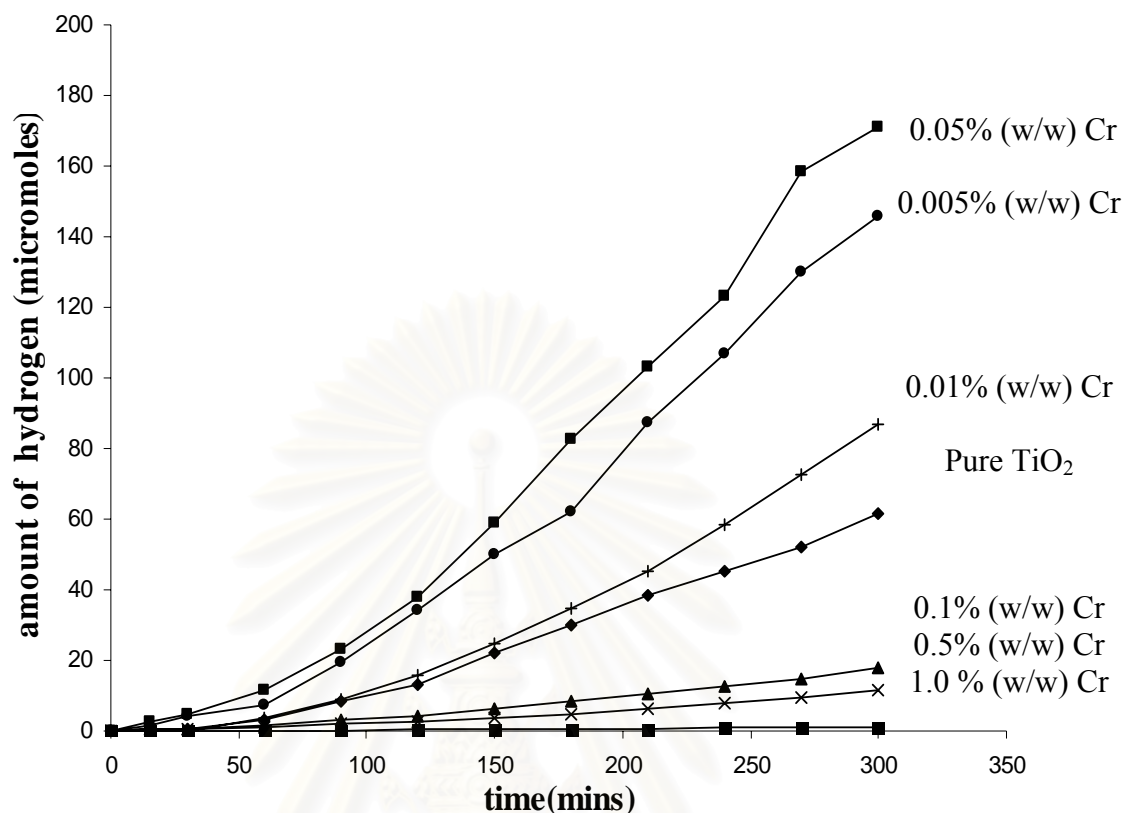


**Figure 5.11** Amount of hydrogen produced from photocatalytic water splitting over titanium dioxide loaded with various amount of chromium.

## 5.2 Properties and photocatalytic activity of titanium dioxide loaded with chromium and 1 % (w/w) platinum.

### 5.2.1 Crystallite phase and size

The phase identification of titanium dioxide was based on the results from X-ray diffraction analysis (XRD). The XRD patterns of various titanium dioxides loaded with chromium and 1 % (w/w) platinum samples were displayed in Figure 5.12. The diffraction peaks at  $2\theta$  values of  $26^\circ$ ,  $37^\circ$ ,  $48^\circ$ ,  $55^\circ$ ,  $56^\circ$ ,  $62^\circ$ ,  $69^\circ$ ,  $71^\circ$ , and  $75^\circ$  indicated that titanium dioxide was primarily in the anatase phase [Suriye et al., 2007]. Small amounts of brookite and rutile were detected in some samples. The average crystallite size of titanium dioxide was estimated from the line broadening of (101) diffraction peak using the Scherrer's equation. The average crystallite size of pure titanium dioxide was approximately 6.2 nm. The crystallite size grew slightly

upon the addition of chromium and platinum, probably due to the calcination performed after metal deposition.

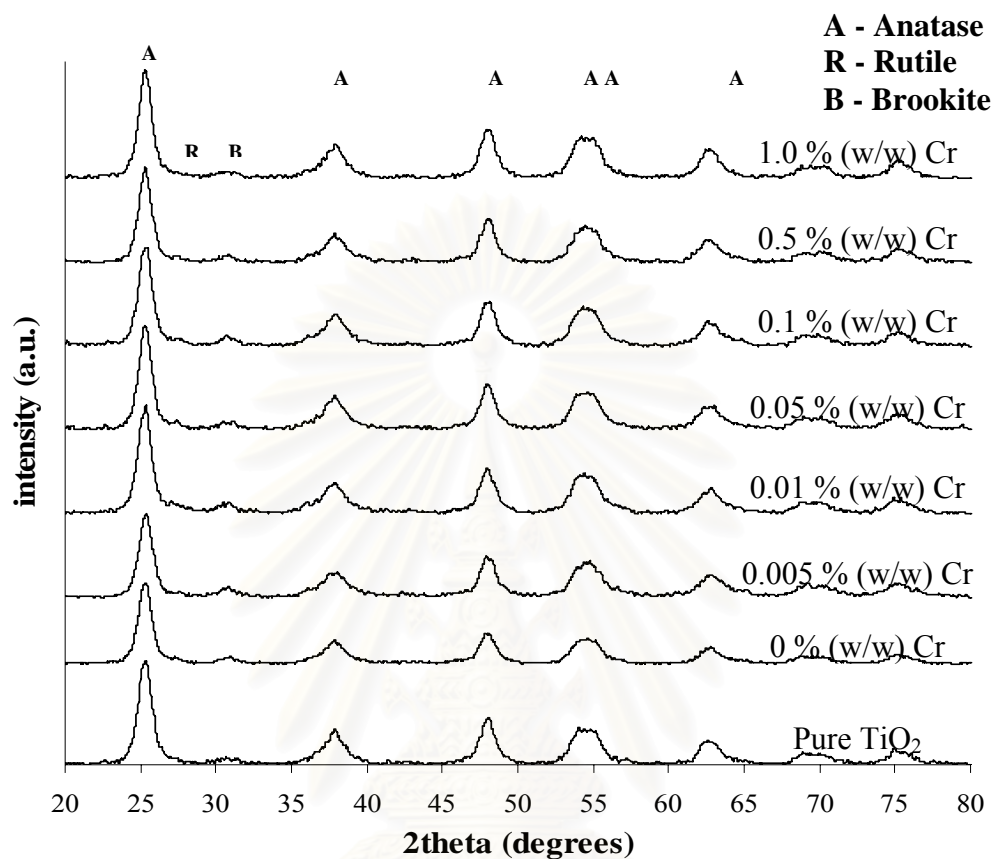


**Figure 5.12** XRD patterns of titanium dioxide loaded with various amount of chromium and 1.0 % (w/w) platinum.

### 5.2.2 Specific surface area

Specific surface areas of the catalysts were determined from nitrogen adsorption isotherms and were displayed in Table 5.4. Pure titanium dioxide possessed the largest specific surface areas. Upon addition of chromium and platinum, specific surface area decreased. However, the amount of chromium loading appeared to have no significant effects on specific surface area of the catalysts.

**Table 5.4** Crystallite size and specific surface area of titanium dioxide with various amounts of Cr and 1.0 % (w/w) Pt loading.

<b>Cr loading (% (w/w))</b>	<b>Crystallize size (nm)</b>	<b>Surface area (m<sup>2</sup>/g)</b>
Pure TiO <sub>2</sub>	6.2	141.1
0	8.1	104.8
0.005	7.6	94.2
0.01	8.0	97.1
0.05	8.0	95.4
0.1	7.3	103.0
0.5	8.0	104.7
1.0	8.7	109.0

### 5.2.3 Metal content

Percentages of chromium and platinum on titanium dioxide catalysts were determined by Inductively coupled plasma atomic emission spectroscopy (ICP-AES). The chromium and 1 % (w/w) platinum content in various catalyst samples were listed in Table 5.5. The chromium content that was determined ICP-AES was lower than the expected chromium content that was calculated for use during the impregnation step. This discrepancy could be a result of incomplete digestion of ICP-AES sample and uneven distribution of metal on titanium dioxide.

**Table 5.5** Chromium and 1 % (w/w) platinum content as measured from ICP-AES, on titanium dioxide loaded with various amount of chromium.

<b>Calculated Cr loading (% (w/w))</b>	<b>Measured Cr content (% (w/w))</b>	<b>Measured Pt content (% (w/w))</b>
0 % (w/w) Cr	0	0.758
0.005 % (w/w) Cr	0.004	0.722
0.01 % (w/w) Cr	0.009	0.735
0.05 % (w/w) Cr	0.024	0.759
0.1 % (w/w) Cr	0.067	0.704
0.5 % (w/w) Cr	0.178	0.758
1.0 % (w/w) Cr	0.451	0.717

### 5.2.4 Light absorption characteristics

UV-visible light absorption characteristics of various titanium dioxides loaded with chromium and 1 % (w/w) platinum were presented in Figure 5.13. A steep drop in the absorbance at a wavelength longer than 387 nm was assigned to the intrinsic band gap absorption of anatase titanium dioxide (3.2 eV). Addition of chromium extended the absorption band of titanium dioxide to the visible region, while leaving the intrinsic band gap of anatase titanium dioxide unaffected. For titanium dioxide, the light absorption in the visible region provided a possibility for enhancing the photocatalytic activity of titanium dioxide. The addition of chromium gave rise to a new absorption shoulder appears at around 420 nm to 550 nm due to the formation of the impurity energy level within the bandgap of titanium dioxide. As seen in Figure 5.13, an increase in chromium content and platinum brought about a better absorption in the visible region for titanium dioxide [Anpo and Takeushi, 2003].

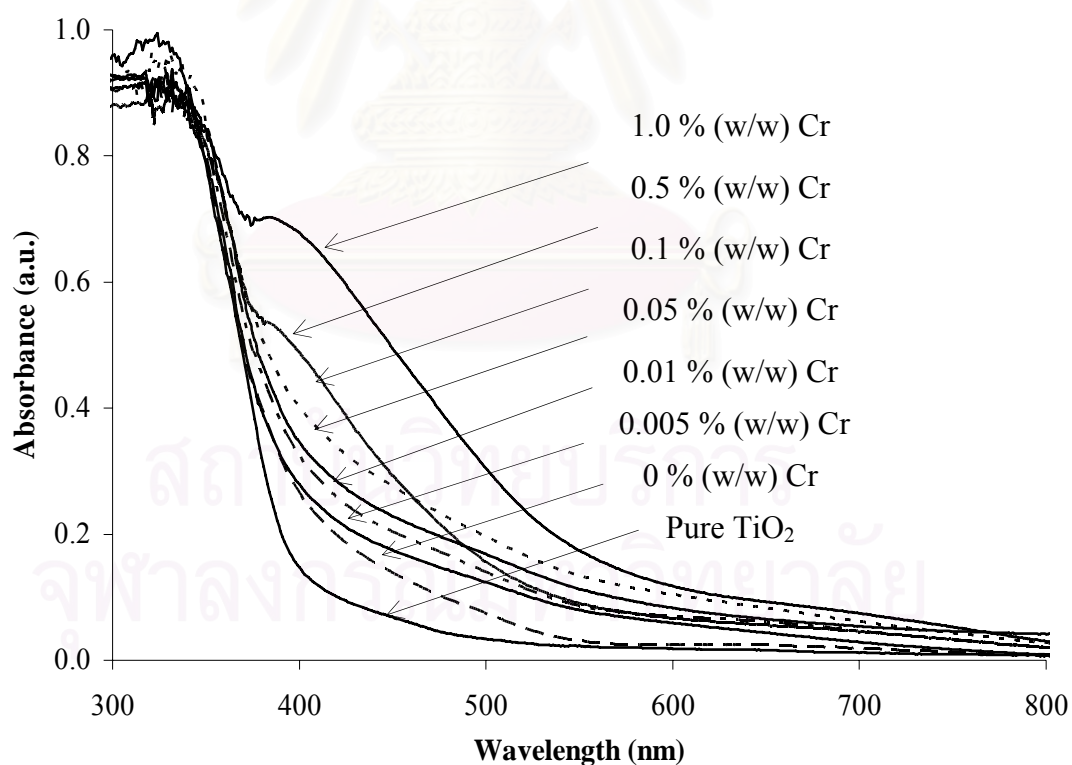


**Figure 5.13** UV-visible absorption characteristics of titanium dioxide loaded with various amount of chromium and 1 % (w/w) platinum.



### 5.2.5 Electron spin resonance spectroscopy

Electron spin resonance spectroscopy (ESR) was performed to determine the amount of  $\text{Ti}^{3+}$  defects in the catalyst. Typical result was displayed in Figure 5.14. The peak observed at the  $g$  value of 1.97 was assigned to  $\text{Ti}^{3+}$  defects. The peak height was proportional to the amount of  $\text{Ti}^{3+}$  in the catalyst. Table 5.6 listed the peak height per unit surface area of various titanium dioxide samples that were loaded with chromium and 1% (w/w) Pt. From Table 5.6, the amount of  $\text{Ti}^{3+}$  (or the peak height) increased when the chromium content was raised. The higher amount of Cr loading may damage the surface of titanium dioxide and form more  $\text{Ti}^{3+}$ .

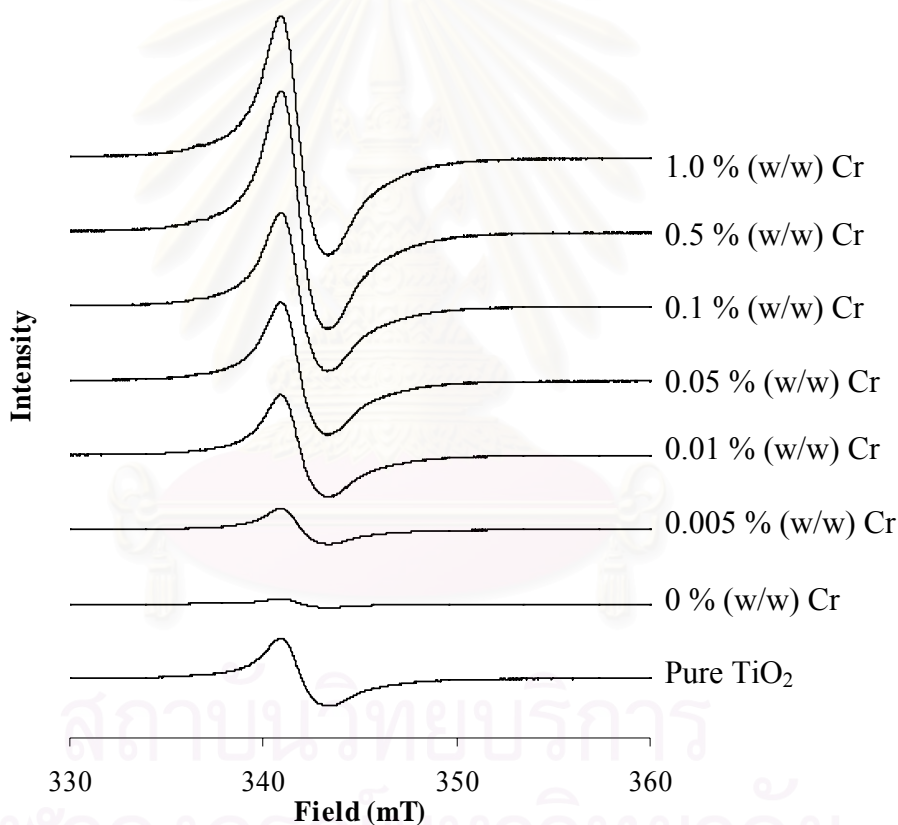


**Figure 5.14** ESR results of titanium dioxide loaded with various amount of Cr and 1% (w/w) Pt.

**Table 5.6** Peak heights per unit surface area, as determined from ESR measurement, for titanium dioxide loaded with various amount of Cr and 1% (w/w) Pt.

<b>Cr loading (% (w/w))</b>	<b>Peak height per unit surface area (1/m<sup>2</sup>)</b>
Pure TiO <sub>2</sub>	70.13
0	1.72
0.005	6.99
0.01	103.17
0.05	141.78
0.1	155.42
0.5	494.23
1.0	681.09

#### 5.2.6 Photoluminescence measurement

Photoluminescence emission spectrum was used to investigate the efficiency of charge carrier trapping, immigration, and transfer; and to understand the fate of electrons and holes in titanium dioxide since photoluminescence emission resulted from the recombination of free carriers. Figures 5.15 displayed the photoluminescence spectra for the catalysts that were excited by irradiation with a wavelength of 350 nm at room temperature. Two main emission peaks were observed at wavelengths of 402 and 458 nm, which corresponded to band gap energies of 3.1 and 2.7 eV, respectively. The first emission peak was ascribed to the emission of band gap transition (or the recombination of photogenerated electrons and holes) at a wavelength of 402 nm. The second emission peak was ascribed to the emission signal originated from the defects levels in the band gap, such as oxygen vacancies formed during sample preparation at wavelengths of 458 nm. The oxygen vacancies were generated because of partially incomplete crystallization [Zhao et al., 2007]. The variation in photoluminescence emission spectrum intensity resulted from the change of defect state on the shallow level of the titanium dioxide surface [Zhao and Yu, 2006]. Figure 5.15 revealed that the photoluminescence signal of pure titanium dioxide was the highest among all the

samples. Upon addition of chromium (from 0.005 % (w/w), 0.05 % (w/w), and 0.01% (w/w), respectively), photoluminescence signals were decreased respectively.

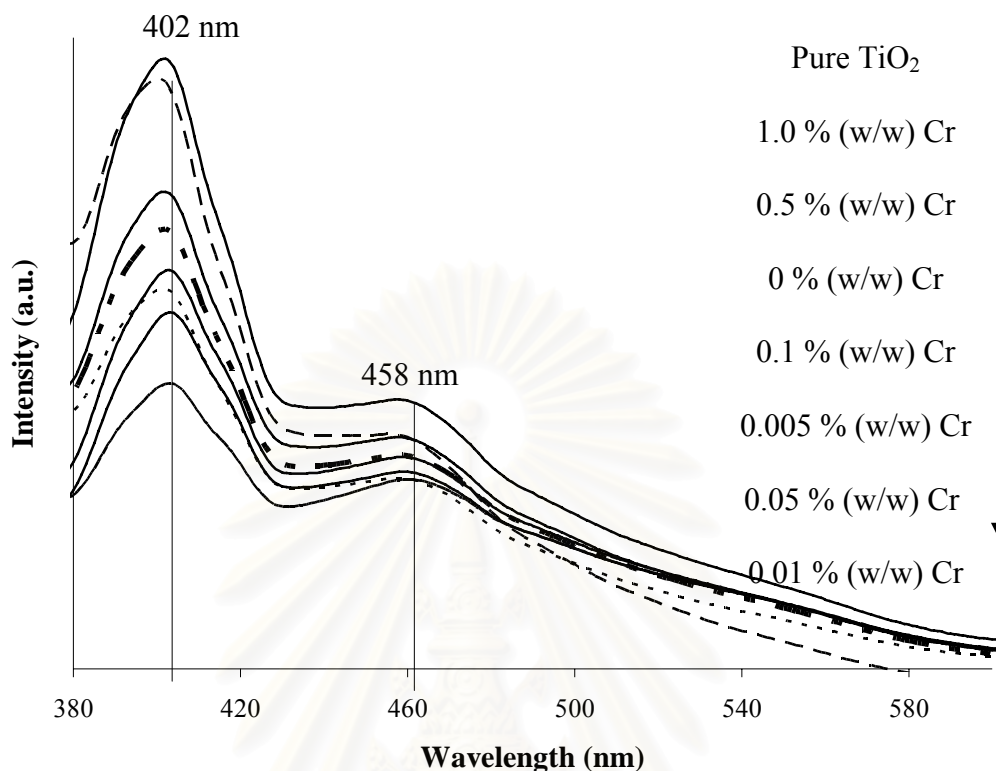


**Figure 5.15** Photoluminescence emission signals of titanium dioxide loaded with various amount of chromium and 1 % (w/w) platinum.

When the chromium content exceeded 0.05 % (w/w), the photoluminescence signals increased back up again. It can be noticed that 0.01 % (w/w) chromium loaded on titanium dioxide shows the lowest photoluminescence signal.

### 5.2.7 Transmission electron microscopy (TEM)

Transmission electron micrographs of  $\text{TiO}_2$  loaded with 1 % (w/w) Cr and 1 % (w/w) Pt were shown in Figure 5.16. TEM were performed in order to physically measure the size of the Cr and Pt clusters. However, the Cr and Pt clusters were not observed because of low Cr loading (less than 1 % (w/w)). Furthermore, the average particle size of  $\text{TiO}_2$  was obtained from the TEM images of the both samples. The average crystallite sizes of pure  $\text{TiO}_2$  and  $\text{TiO}_2$  loaded with 1 % (w/w) Cr and Pt were 6.2 nm and 8.6 nm, respectively. These results were good agreement with the average crystallite sizes that were determined from XRD analysis (see Table 5.4)

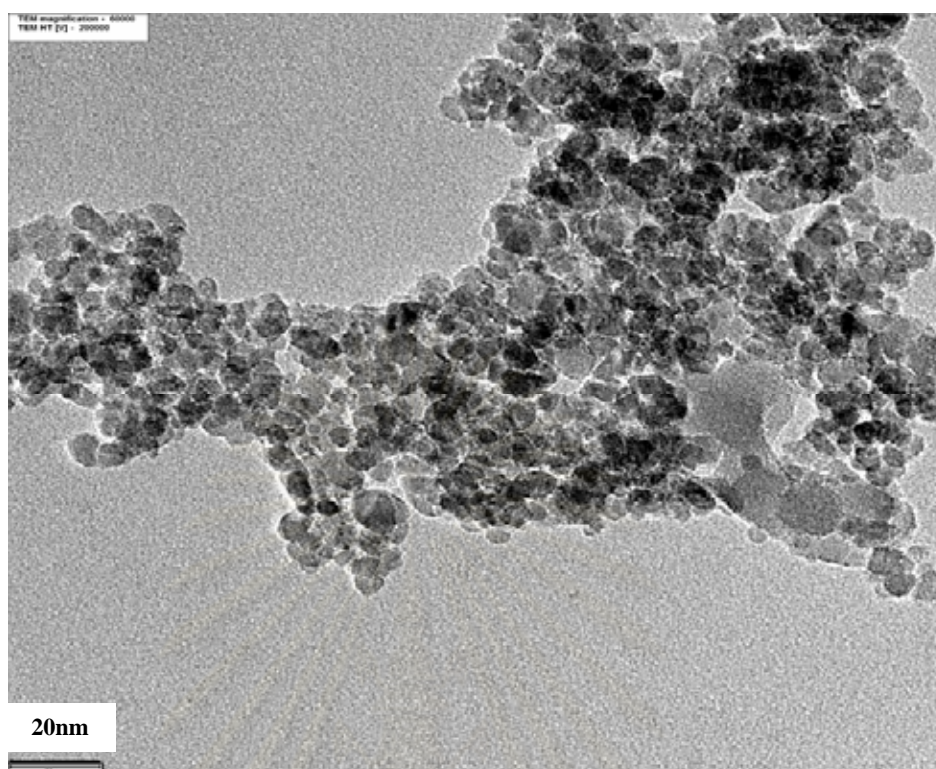


**Figure 5.16** TEM micrographs of titanium dioxide loaded with various amount of chromium and 1.0 % (w/w) platinum.

### 5.2.8 Photocatalytic activity

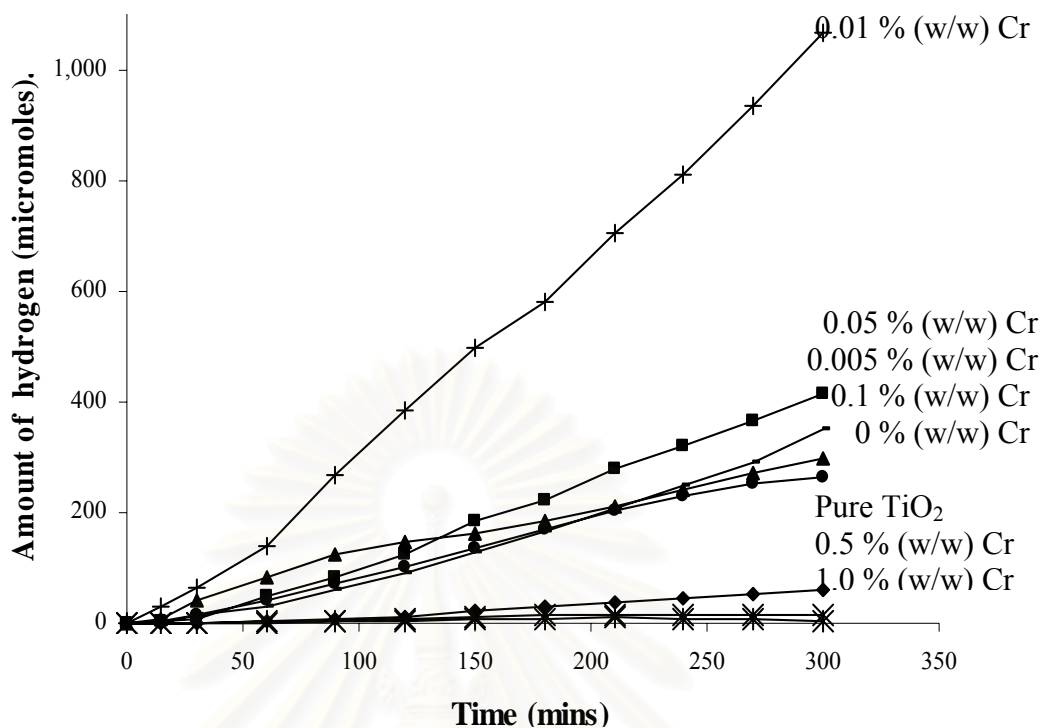
From researches the addition of noble metals to  $\text{TiO}_2$  was found to be beneficial for the photocatalysis. The photocatalytic with noble metals on  $\text{TiO}_2$  exemplifies. Ni and coworker [2005] proposed that noble metals (Pt, Rh, Pd, Au, Ni, Cu and Ag) have been to be very effective for enhancement of  $\text{TiO}_2$  photocatalysis. As the Fermi levels of these noble metals are lower than that of titania, photo excited electrons can be transferred from conduction band to metal particles deposited on the surface of  $\text{TiO}_2$  while photo-generated valence band holes remain on the titanium dioxide. Jin and coworker [2006] proposed that enhancement of quantum yield was achieved via noble metal loading and subsequent dye sensitization of noble metal/ $\text{TiO}_2$ .  $\text{H}_2$  evolution was enhanced with the increase of the metal loading, which have resulted from the strong adsorption of eosin on the loading metal. Anpo and coworker [2003] proposed that the noble metal particles accumulated electrons and their Fermi levels shifted closer to the conduction band of  $\text{TiO}_2$ . Chen and coworker [2007]

studied photocatalytic reaction of methanol on Pt/TiO<sub>2</sub>. Platinum on TiO<sub>2</sub> was trapped the excited electrons, and the adsorbate species from methanol capture the holes, which are important for improving the yield of long-lived electrons. These long-lived electrons decay on the millisecond to second scale in Pt/TiO<sub>2</sub>, and the decays correspond to the electron consumption process for H<sub>2</sub> generation. Bamwenda and coworker [1995] compared hydrogen production from water-ethanol solution using Au-loaded TiO<sub>2</sub> and Pt-loaded TiO<sub>2</sub> as photocatalysts. Different metal particle deposition methods, such as deposition-precipitation, impregnation and photodeposition were tested. It was found that loading of Pt worked better than loading of Au. Furthermore, Au loading prepared by photodeposition worked better than deposition-precipitation and impregnation. The variations might be explained by the better contact with TiO<sub>2</sub> active sites for photodeposition method. However, Pt-loaded TiO<sub>2</sub> was found to be less sensitive to the preparation methods. The possibility of electron-hole recombination from reviews in efficient separation and stronger photocatalytic reactions with noble metal loaded on TiO<sub>2</sub>.

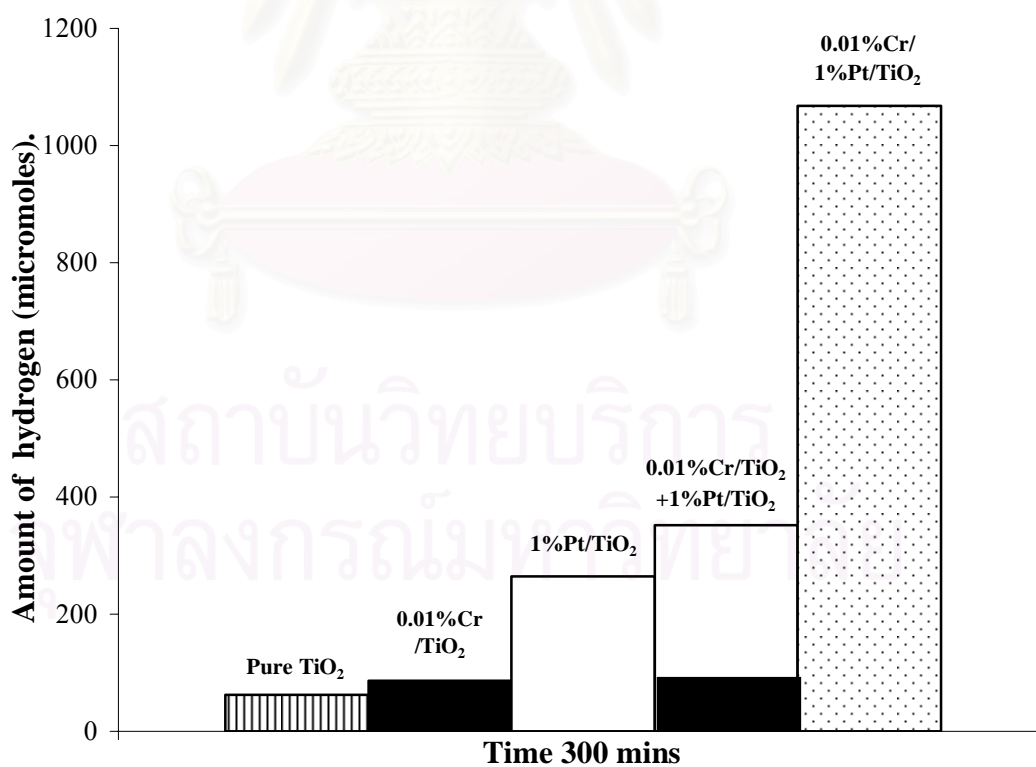
Photocatalytic activities of doped with 1 % (w/w) platinum and various amount of chromium loading on titanium dioxide were quantified by the amount of hydrogen gas produced from the photoreactor. From Figure 5.17 titanium dioxide loaded with 0.01 % (w/w) possessed the highest activity. This result agreed with result from photoluminescence measurement. The order of decreasing activity (0.01 % (w/w), 0.05 % (w/w), and 0.005 % (w/w), and pure titanium dioxide was the same as the order of increasing photoluminescence signals (see Figure 5.15).

Figure 5.18 compared the amount of hydrogen gas that was produced by photocatalytic water splitting over pure titanium dioxide, titanium dioxide loaded with chromium alone, titanium dioxide loaded with platinum alone, and titanium dioxide loaded with chromium and platinum after 300 minutes of reaction times. The amount of hydrogen produced from titanium dioxide that was loaded with both chromium and platinum was significantly higher than the sum of the amount of hydrogen produced from titanium dioxide that was loaded with either metal alone. This result suggested that the loading of chromium and platinum together gave rise to a synergy that significantly enhanced the photocatalytic activity of the catalyst.





**Figure 5.17** Amount of hydrogen produced from photocatalytic water splitting over titanium dioxide loaded with various amount of Cr and 1 % (w/w) Pt.



**Figure 5.18** Amount of hydrogen produced by pure TiO<sub>2</sub> and various amounts of metals in photocatalytic was compared at time 300 mins.

### 5.3 Properties and photocatalytic activity of titanium dioxide loaded with chromium and 1 % (w/w) rhodium.

#### 5.3.1 Crystallite phase and size

The phase identification of titanium dioxide was based on the results from X-ray diffraction analysis (XRD). The XRD patterns of various titanium dioxides loaded with chromium and 1 % (w/w) rhodium samples were displayed in Figure 5.19. The diffraction peaks at  $2\theta$  values of  $26^\circ$ ,  $37^\circ$ ,  $48^\circ$ ,  $55^\circ$ ,  $56^\circ$ ,  $62^\circ$ ,  $69^\circ$ ,  $71^\circ$ , and  $75^\circ$  indicated that titanium dioxide was primarily in the anatase phase [Suriye et al., 2007]. Small amounts of brookite and rutile were detected in some samples. The average crystallite size of titanium dioxide was estimated from the line broadening of (101) diffraction peak using the Scherrer's equation. The average crystallite size of pure titanium dioxide was approximately 6.2 nm. The crystallite size grew slightly upon the addition of chromium and rhodium, probably due to the calcination performed after metal deposition.

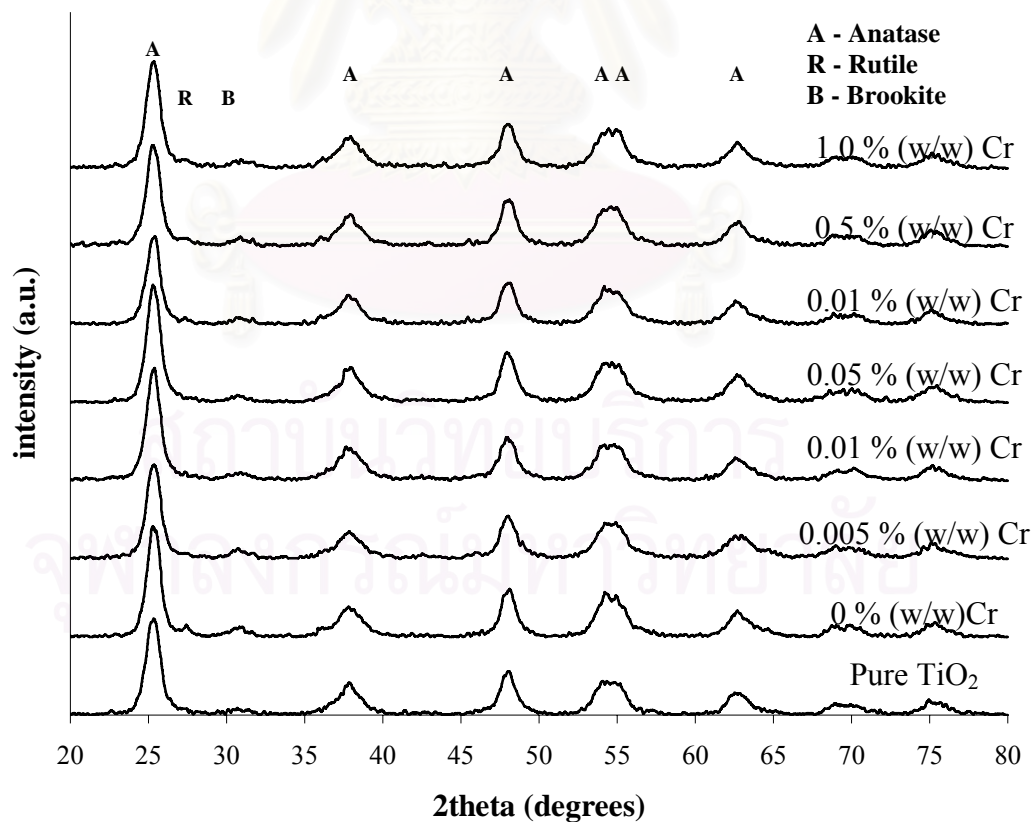


**Figure 5.19** XRD patterns of titanium dioxide loaded with various amount of chromium and 1.0 % (w/w) rhodium.

### 5.3.2 Specific surface area

Specific surface areas of the catalysts were determined from nitrogen adsorption isotherms and were displayed in Table 5.7. Pure titanium dioxide possessed the largest specific surface areas. Upon addition of chromium and rhodium, specific surface area decreased. However, the amount of chromium loading appeared to have no significant effects on specific surface area of the catalysts.

### 5.3.3 Metal content

Percentages of chromium on titanium dioxide catalysts were determined by Inductively coupled plasma atomic emission spectroscopy (ICP-AES). The chromium and 1 % (w/w) rhodium content in various catalyst samples were listed in Table 5.8. The chromium content that was determined ICP-AES was lower than the expected chromium content that was calculated for use during the impregnation step. This discrepancy could be a result of incomplete digestion of ICP-AES sample and uneven distribution of metal on titanium dioxide.

**Table 5.7** Crystallite size and specific surface area of titanium dioxide with various amounts of Cr and 1.0 % (w/w) rhodium loading.

Cr loading (% (w/w))	Crystallizes size (nm)	Surface areas (m <sup>2</sup> /g)
Pure TiO <sub>2</sub>	6.2	141.1
0	7.7	96.6
0.005	7.8	90.9
0.01	7.8	105.9
0.05	8.3	92.1
0.1	7.7	99.8
0.5	7.9	95.9
1.0	7.6	100.9

**Table 5.8** Chromium and 1 % (w/w) rhodium content as measured from ICP-AES, on titanium dioxide loaded with various amount of chromium and 1.0 % (w/w) rhodium.

<b>Calculated Cr loading (% (w/w))</b>	<b>Measured Cr content (% (w/w))</b>
0% (w/w) Cr	0
0.005% (w/w) Cr	0.003
0.01% (w/w) Cr	0.007
0.05% (w/w) Cr	0.022
0.1% (w/w) Cr	0.084
0.5% (w/w) Cr	0.244
1.0% (w/w) Cr	0.469

#### 5.3.4 Light absorption characteristics

UV-visible light absorption characteristics of various titanium dioxides loaded with chromium and 1 % (w/w) rhodium were presented in Figure 5.20. A steep drop in the absorbance at a wavelength longer than 387 nm was assigned to the intrinsic band gap absorption of anatase titanium dioxide (3.2 eV). Addition of chromium extended the absorption band of titanium dioxide to the visible region, while leaving the intrinsic band gap of anatase titanium dioxide unaffected. For titanium dioxide, the light absorption in the visible region provided a possibility for enhancing the photocatalytic activity of titanium dioxide. The addition of chromium gave rise to a new absorption shoulder appears at around 420 nm to 550 nm due to the formation of the impurity energy level within the bandgap of titanium dioxide. As seen in Figure 5.20, an increase in chromium content and rhodium brought about a better absorption in the visible region for titanium dioxide [Anpo and Takeushi, 2003].

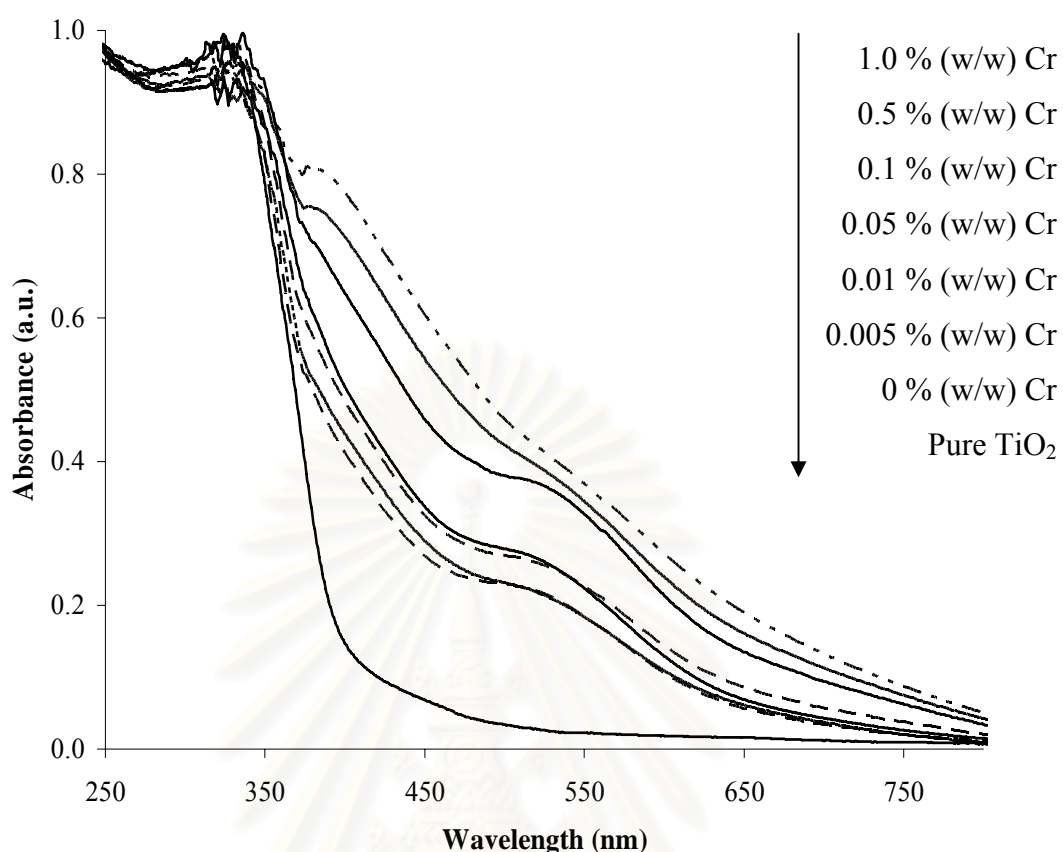


**Figure 5.20** UV-visible absorption characteristics of titanium dioxide loaded with various amount of chromium and 1 % (w/w) rhodium.

### 5.3.5 Electron spin resonance spectroscopy

Electron spin resonance spectroscopy (ESR) was performed to determine the amount of  $\text{Ti}^{3+}$  defects in the catalyst. Typical result was displayed in Figure 5.21. The peak observed at the  $g$  value of 1.97 was assigned to  $\text{Ti}^{3+}$  defects. The peak height was proportional to the amount of  $\text{Ti}^{3+}$  in the catalyst. Table 5.9 listed the peak height per unit surface area of various titanium dioxide samples that were loaded with chromium and 1% (w/w) Rh. From Table 5.9, the amount of  $\text{Ti}^{3+}$  (or the peak height) increased when the chromium content was raised. The higher amount of Cr loading may damage the surface of titanium dioxide and form more  $\text{Ti}^{3+}$ .



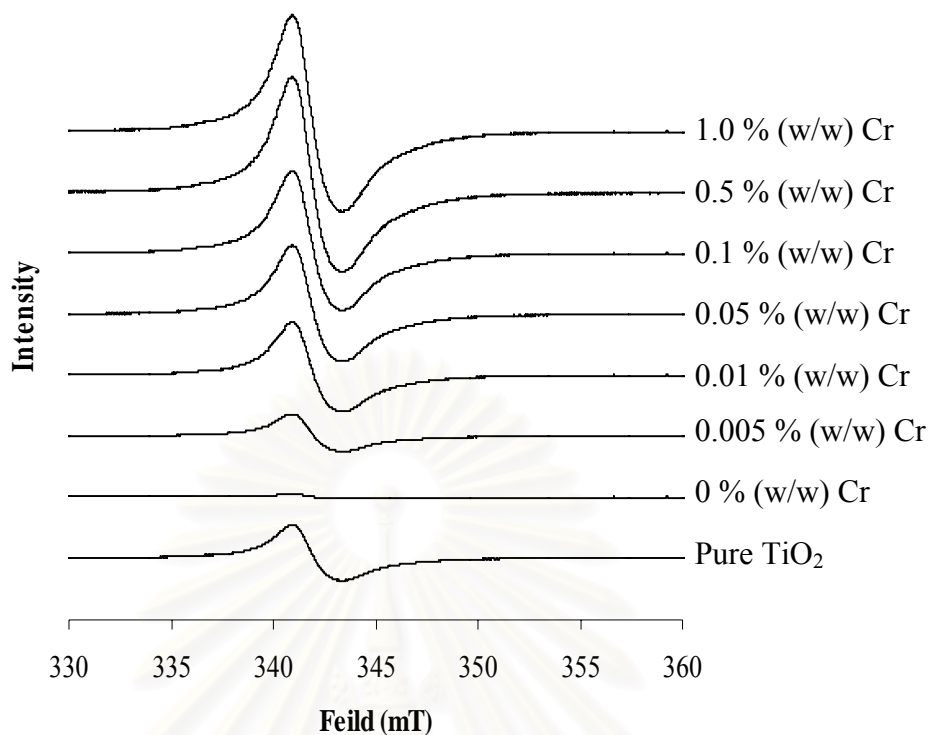


**Figure 5.21** Peak height ESR result of titanium dioxide loaded with various amount of Cr and 1% (w/w) Rh.

**Table 5.9** Peak heights per unit surface area, as determined from ESR measurement, result of titanium dioxide loaded with various amount of Cr and 1% (w/w) Rh.

Cr loading (% (w/w))	Peak height per unit surface area (Peak height / $S_{BET}$ )
Pure TiO <sub>2</sub>	70.13
0	1.369431
0.005	35.42354
0.01	114.3332
0.05	302.8744
0.1	374.7815
0.5	794.4008
1.0	811.5874

### 5.3.6 Photoluminescence measurement

Photoluminescence emission spectrum was used to investigate the efficiency of charge carrier trapping, immigration, and transfer; and to understand the fate of electrons and holes in titanium dioxide since photoluminescence emission resulted from the recombination of free carriers. Figures 5.22 displayed the photoluminescence spectra for the catalysts that were excited by irradiation with a wavelength of 350 nm at room temperature. Two main emission peaks were observed at wavelengths of 402 and 458 nm, which corresponded to band gap energies of 3.1 and 2.7 eV, respectively. The first emission peak was ascribed to the emission of band gap transition (or the recombination of photogenerated electrons and holes) at a wavelength of 402 nm. The second emission peak was ascribed to the emission signal originated from the defects levels in the band gap, such as oxygen vacancies formed during sample preparation at wavelengths of 458 nm. The oxygen vacancies were generated because of partially incomplete crystallization [Zhao et al., 2007]. The variation in photoluminescence emission spectrum intensity resulted from the change of defect state on the shallow level of the titanium dioxide surface [Zhao and Yu, 2006]. Figure 5.22 revealed that the photoluminescence signal of pure titanium dioxide was the highest among all the samples. Upon addition of chromium (from 0.005 % (w/w), 0.05 % (w/w), and 0.01% (w/w), respectively), photoluminescence signals were decreased respectively. When the chromium content exceeded 0.05 % (w/w), the photoluminescence signals increased back up again. It can be noticed that 0.01 % (w/w) chromium loaded on titanium dioxide shows the lowest photoluminescence signal.

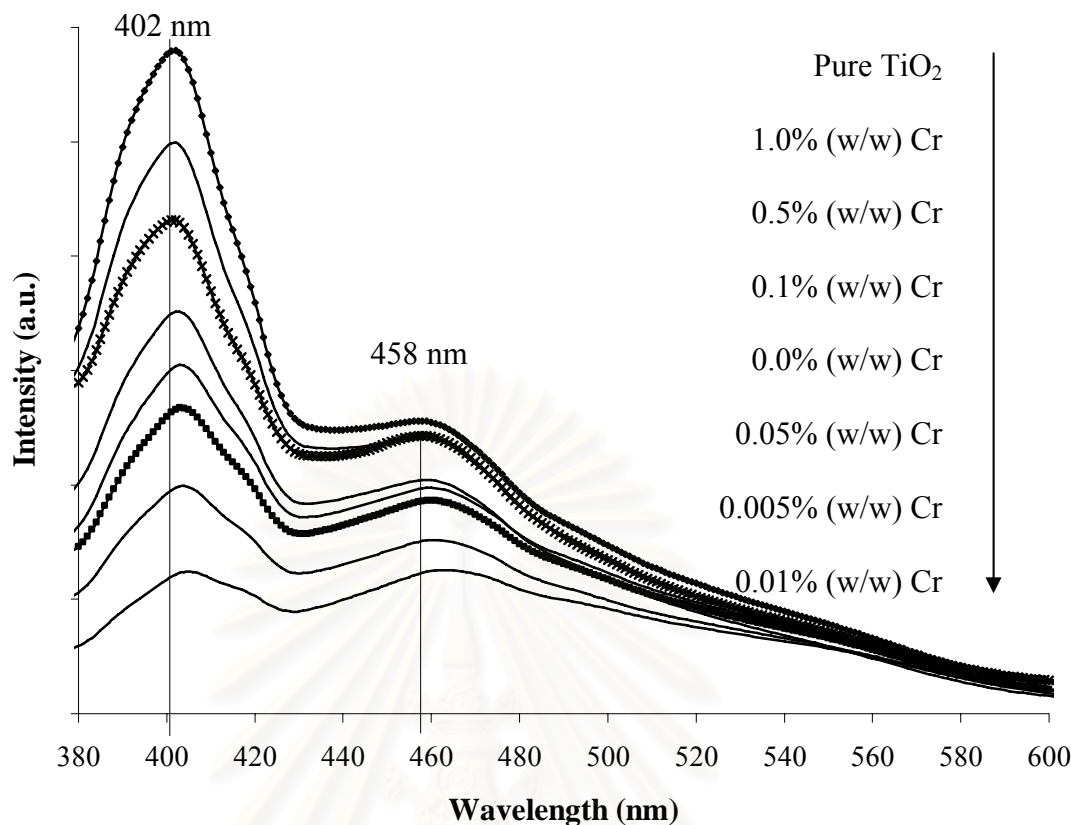


**Figure 5.22** Photoluminescence emission signals of titanium dioxide loaded with various amount of chromium and 1 % (w/w) platinum.

### 5.3.7 Photocatalytic activity

From researches the addition of noble metals to  $\text{TiO}_2$  was found to be beneficial for the photocatalysis. The photocatalytic with noble metals on  $\text{TiO}_2$  exemplifies. Ni and coworker [2005] proposed that noble metals (Pt, Rh, Pd, Au, Ni, Cu and Ag) have been to be very effective for enhancement of  $\text{TiO}_2$  photocatalysis. As the Fermi levels of these noble metals are lower than that of titania, photo excited electrons can be transferred from conduction band to metal particles deposited on the surface of  $\text{TiO}_2$  while photo-generated valence band holes remain on the titanium dioxide. Jin and coworker [2006] proposed that enhancement of quantum yield was achieved via noble metal loading and subsequent dye sensitization of noble metal/ $\text{TiO}_2$ .  $\text{H}_2$  evolution was enhanced with the increase of the metal loading, which have resulted from the strong adsorption of eosin on the loading metal. Anpo and coworker [2003] proposed that the noble metal particles accumulated electrons and their Fermi levels shifted closer to the conduction band of  $\text{TiO}_2$ . The possibility of electron-hole

recombination from reviews in efficient separation and stronger photocatalytic reactions with noble metal loaded on  $\text{TiO}_2$ .

Photocatalytic activities of doped with 1 % (w/w) rhodium and various amount of chromium loading on titanium dioxide were quantified by the amount of hydrogen gas produced from the photoreactor. From Figure 5.23 titanium dioxide loaded with 0.01 % (w/w) possessed the highest activity. This result agreed with result from photoluminescence measurement. The order of decreasing activity (0.01 % (w/w), 0.05 % (w/w), and 0.005 % (w/w), and pure titanium dioxide was the same as the order of increasing photoluminescence signals (see Figure 5.15).

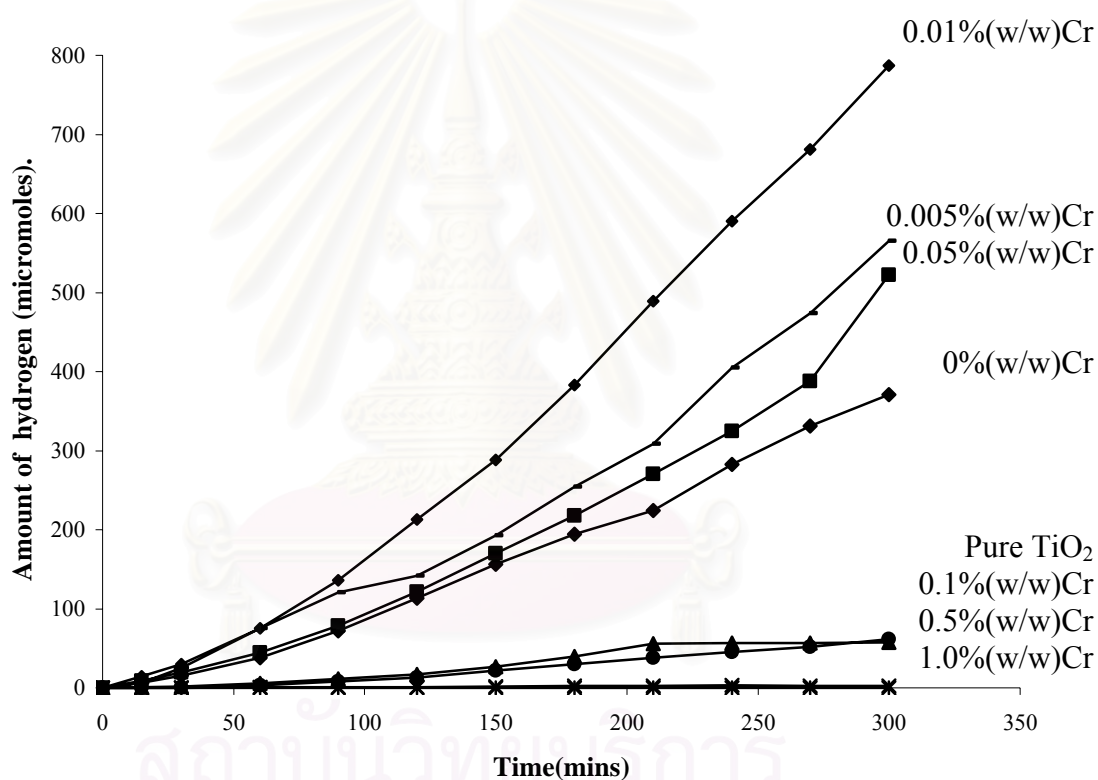


**Figure 5.23** Amount of hydrogen produce from photocatalytic water splitting over titanium dioxide loaded with various amount of Cr and 1 % (w/w) Rh.

Figure 5.24 compared the amount of hydrogen gas that was produced by photocatalytic water splitting over pure titanium dioxide, titanium dioxide loaded with chromium alone, titanium dioxide loaded with rhodium alone, and titanium dioxide loaded with chromium and rhodium after 300 minutes of reaction times. The amount of hydrogen produced from titanium dioxide that was loaded with both chromium and

rhodium was significantly higher than the sum of the amount of hydrogen produced from titanium dioxide that was loaded with either metal alone. This result suggested that the loading of chromium and rhodium together gave rise to a synergy that significantly enhanced the photocatalytic activity of the catalyst.

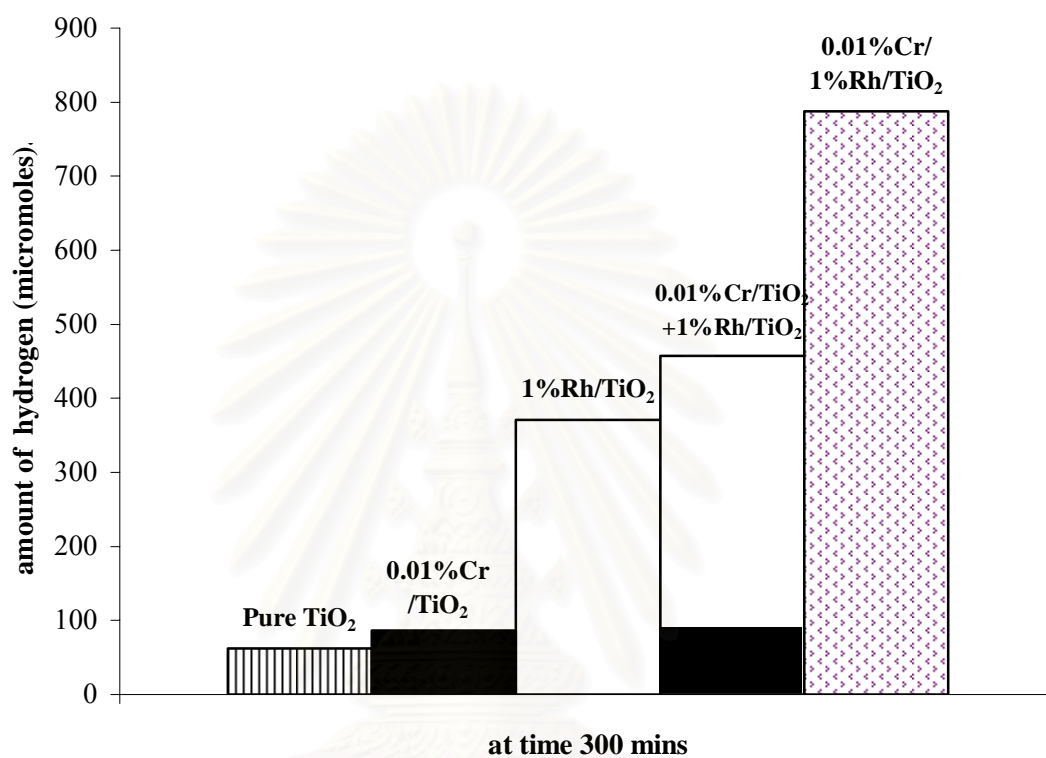


**Figure 5.24** Amount of hydrogen produced by pure TiO<sub>2</sub> and various amounts of metals in photocatalytic was compared at time 300 mins.

สถาบันวิทยบริการ  
จุฬาลงกรณ์มหาวิทยาลัย



## CHAPTER VI

### CONCLUSION AND RECOMMENDATIONS

#### 6.1 Conclusion

Photocatalytic activity of titanium dioxide for water splitting was enhanced by addition of Cr. The highest activity was observed in titanium dioxide loaded with 0.05% (w/w) Cr. To improve the activity further, chromium was added to TiO<sub>2</sub> together with either Pt or Rh. The highest activity was achieved with titanium dioxide that was loaded with 0.01% (w/w) Cr and 1% (w/w) Pt or Rh. The enhanced photocatalytic activities of doped catalysts were attributed to the ability of metals added to prevent recombination of the photogenerated electron/hole pairs, which was evident from the lowering of the photoluminescence signal.

#### 6.2 Recommendations for the future studies

1. The effect of the noble metals (Pt or Rh) on photocatalytic activity as well as optimum loading of Pt and Rh should be studied.
2. The effect of the order of metal loading should be studied.

สถาบันวิทยบริการ  
จุฬาลงกรณ์มหาวิทยาลัย

## REFERENCES

- Anpo, M., and Takeuchi, M. (2003). The design and development of highly reactive titanium oxide photocatalysts operating under visible light irradiation. Journal of Catalysis 216: 505-16.
- Bamwenda, GR., Tsubota, S., Nakamura, T., and Haruta M. (1995). Photoassisted hydrogen production from a water ethanol solution: a comparison of activities of Au-TiO<sub>2</sub> and Pt-TiO<sub>2</sub>. Journal of Photochemistry and Photobiology A: Chemical 89: 177-89.
- Brezova, V., Blazkova, A., Karpinsky, L., Groskova, J., Havlinova, B., Jorik, V., and Ceppan, M. (1997). Phenol decomposition using M<sup>n+</sup>/TiO<sub>2</sub> photocatalysts supported by the sol-gel technique on glass fibres. Journal of Photochemistry and Photobiology A: Chemistry 109: 177-183.
- Chen, T., Feng, Z., Wu, G., Shi, J., Ma, G., Ying, P., and Li, C. (2007). Mechanistic Studies of Photocatalytic Reaction of Methanol for Hydrogen Production on Pt/TiO<sub>2</sub> by in situ Fourier Transform IR and Time-Resolved IR Spectroscopy. Journal of Physical Chemistry C 111: 8005-8014.
- Chen, Y.-F., Lee, C.-Y., Yang, M.-Y., Chiu, H.-T. (2003). The effect of calcination temperature on the crystallinity of TiO<sub>2</sub> nanopowders. Journal of Crystal Growth 247: 363-370.
- Ekou, T., Vicente, A., Lafaye, G., Especel, C., and Marecot, P. (2006). Bimetallic Rh-Ge and Pt-Ge catalysts supported on TiO<sub>2</sub> for citral hydrogenation I. Preparation and characterization of the catalysts. Applied Catalysis A: General 314: 64-72.
- Fuerte, A., Hernandez-Alonso, M. D., Maria, A. J., Martinez-Arias, A., Fernandez-Garcia, M., Conesa, J. C., Soria, J. (2001). Visible light activated nanosized doped-TiO<sub>2</sub> photocatalysts. Chemical Communications 2718-2719.

- Fujishima, A., Hashimoto, K., and Watanabe, T.,  $\text{TiO}_2$  photocatalysis: fundamental and applications. 1<sup>st</sup> ed Tokyo: BKC, 1999.
- Geula, D. and Micha, T. (1993).  $\text{TiO}_2$  Aerogels for Photocatalytic Decontamination of Aquatic Enviroments. Journal of Physical Chemistry 97: 12651-12655.
- Gurunathan, K., Maruthamuthu, P., and Sastri, M. V. C. (1997). Photocatalytic hydrogen production by dye-sensitized  $\text{Pt/SnO}_2$  AND  $\text{Pt/SnO}_2/\text{RuO}_2$  in aqueous methyl viologen solution. International Journal of Hydrogen Energy 22(1): 57-62.
- Ikuma, Y. and Bessho, H. (2006). Effect of Pt concentration on the production of hydrogen by a  $\text{TiO}_2$  photocatalyst. International Journal of Hydrogen Energy 32: 2689-2692
- Jin, Z., Zhang, X., Lu, G., Li S. (2006). Improved quantum yield for photocatalytic hydrogen generation under visible light irradiation over eosin sensitized  $\text{TiO}_2$  - Investigation of different noble metal loading. Journal of Molecular Catalysis A: Chemical 259: 275-280.
- John, MR., Furgals, AJ. and Sammells, AF. (1983). Hydrogen Generatlon by Photocatalytic Oxidation of Glucose by Platinized n- $\text{TiO}_2$  Powder. Journal of Physical Chemistry 87: 801–805.
- Ikeda, S., Sugiyama, N., Pal, B., Marci, G., Palmisano, L., Noguchi, H., Uosaki, K., Ohtani, B. (2001). Photocatalytic activity of transition-metal-loaded titanium(IV) oxide powders suspended in aqueous solutions: Correlation with electron-hole recombination kinetics. Physical Chemistry Chemical Physics 3: 267-273.
- Kida, T., Guan, G. Yamada, N., Ma, T., Kimura, K., and Yoshida, A. (2004). Hydrogen production from sewage sludge solubilized in hot-compressed water

using photocatalyst under light irradiation. International Journal of Hydrogen Energy 29(3): 269-274.

Li, Y., Lu, G., and Li, S. (2003). Photocatalytic production of hydrogen in single component and mixture systems of electron donors and monitoring adsorption of donors by in situ infrared spectroscopy. Chemosphere 52(5): 843-850.

Litter I. M. (1999). Review Heterogeneous photocatalysis Transition metal ions in photocatalytic systems. Applied Catalysis B: Environmental 23: 89-114.

Maeda, K., Teramura, K., Saito, N., Inoue, Y., Domen, K. (2006). Improvement of photocatalytic activity of  $(\text{Ga}_{1-x}\text{Zn}_x)(\text{N}_{1-x}\text{O}_x)$  solid solution for overall water splitting by co-loading Cr and another transition metal. Journal of Catalyst 243: 303-308.

Moon, S. C., Mametsuka, H., Tabata, S., and Suzuki, E. (2000). Photocatalytic production of hydrogen from water using  $\text{TiO}_2$  and B/ $\text{TiO}_2$ . Catalysis Today 58(2-3): 126.

Nada, A. A., Barakat, M. H., Hamed, H. A., Mohamed, N.R., and Veziroglu, T.N. (2005). Studies on the photocatalytic hydrogen production using suspended modified  $\text{TiO}_2$  photocatalysts. International Journal of Hydrogen Energy 30: 687-691.

Ni, M., Leung, M. K. H., Leung, Y.C. D., Sumathy, K. (2005). A review and recent developments in photocatalytic water-splitting using  $\text{TiO}_2$  for hydrogen production. Renewable and Sustainable Energy Reviews 11: 401-425.

Rajesh J. T., Ramchandra G. K., and Raksh. V. J., (2006). Transition Metal Ion Impregnated Mesoporous  $\text{TiO}_2$  for Photocatalytic Degradation of Organic Contaminants in Water. Industrial & Engineering Chemistry Research 45: 5231-5238.

- Sakata, T., Kawai, T., and Hashimoto, K. (1982). Photochemical diode model of Pt/TiO<sub>2</sub> particle and its photocatalytic activity. Chemical Physics Letters 88(1): 50-54.
- Sakthivel, S.; Shankar, MV.; Palanichamy, M.; Arabindoo, B.; Bahnemann, DW.; Murugesan, V. (2004). Enhancement of photocatalytic activity by metal deposition: characterisation and photonic efficiency of Pt, Au and Pd deposited on TiO<sub>2</sub> catalyst. Water Research 38: 3001-3008.
- Sreethawong, T., Puangpetch, T., Chavadej, S., Yoshikawa, S. (2007). Quantifying influence of operational parameters on photocatalytic H<sub>2</sub> evolution over Pt-loaded nanocrystalline mesoporous TiO<sub>2</sub> prepared by single-step sol-gel process with surfactant template. Journal of Power Sources 165: 861–869.
- Su, C., Hong, B., and Tseng, C. (2004). Sol-gel preparation and photocatalysis of titanium dioxide. Catalyst Today 96: 119-126.
- Suriye, K., Praserttham, P., and Jongsomjit, B. (2007). Control of Ti<sup>3+</sup> surface defect on TiO<sub>2</sub> nanocrystal using various calcination atmospheres as the first step for surface defect creation and its application in photocatalysis. Applied Surface Science 253: 3849–3855.
- Wu, C. G., Chao, C. C., and Kuo, F. T. (2004). Enhancement of the photo catalytic performance of TiO<sub>2</sub> catalysts via transition metal modification. Catalysis Today 97: 103–112.
- Wu, N. L., Lee, M. S., Pon, Z. J., and Hsu, J. Z. (2004). Effect of calcination atmosphere on TiO<sub>2</sub> photocatalysis in hydrogen production from methanol/water solution. Journal of Photochemistry and Photobiology a-Chemistry 163(1-2): 277-280.
- Zhao, L., and Yu, J. (2006). Controlled synthesis of highly dispersed TiO<sub>2</sub> nanoparticles using SBA-15 as hard template. Journal of Colloid and Interface Science 304: 84-91.



Zhao, Y., Li, C., Liu, X., Gu, F., Jiang, H., Shao, W., Zhang, L., He, Y. (2007). Synthesis and optical properties of TiO<sub>2</sub> nanoparticles. Materials Letters 61: 79-83.

Zhu, J., Deng, Z., Chen, F., Zhang, J., Chen, H., Anpo, M., Huang, J., and Zhang, L. (2006). Hydrothermal doping method for preparation of Cr<sup>3+</sup>-TiO<sub>2</sub> photocatalysts with concentration gradient distribution of Cr<sup>3+</sup>. Applied Catalysis B: Environmental 62: 329-335.



สถาบันวิทยบริการ  
จุฬาลงกรณ์มหาวิทยาลัย



**APPENDICES**

สถาบันวิทยบริการ  
จุฬาลงกรณ์มหาวิทยาลัย

## APPENDIX A

### CALCULATION FOR CATALYST PREPARATION

Calculation for the amount of chromium precursor to be used during the incipient wetness impregnation method is shown below.

Reagent: - Chromium (III) nitrate nonohydrate ( $\text{Cr}(\text{NO}_3)_3 \cdot 9\text{H}_2\text{O}$ )  
Molecular weight = 400.14 g/mol  
- Support: Titania [ $\text{TiO}_2$ ]

**Example** Calculation for the preparation of 1 % (w/w) Cr on  $\text{TiO}_2$

Based on 100 g of catalyst used, the composition of the catalyst is

Chromium = 1 g  
Titania = 100-1 = 99 g

For 5 g of titania

Chromium required =  $5 \times (1/99)$  = 0.0505 g

Chromium 0.0505 g was prepared from  $\text{Cr}(\text{NO}_3)_3 \cdot 9\text{H}_2\text{O}$  and molecular weight of Cr is 52.00 g/mol

$$\begin{aligned} \text{Cr}(\text{NO}_3)_3 \cdot 9\text{H}_2\text{O} \text{ required} &= \frac{\text{MW of } \text{Cr}(\text{NO}_3)_3 \cdot 9\text{H}_2\text{O} \times \text{Chromium required}}{\text{MW of Cr}} \\ &= (400.14/52.00) \times 0.0505 = 0.3886 \text{ g} \end{aligned}$$

Since the pore volume of the titania support is 0.4 ml/g, the total volume was observed from drop pure de-ionized water on the titania support. The total volume of impregnation solution was used about 1.2 ml. By the requirement of the incipient wetness impregnation method, the volume of de-ionized water used for dissolution of precursor must equal pore volume of the support.

## APPENDIX B

### CALCULATION OF THE CRYSTALLITE SIZE

Calculation of the crystallite size by Debye-Scherrer equation

The crystallite size is calculated from the half-height width of the diffraction peak of XRD pattern using the Debye-Scherrer equation.

From Scherrer equation:

$$D = \frac{K\lambda}{\beta \cos \theta} \quad (\text{A.1})$$

- where
- D = Crystallite size, Å
  - K = Crystallite-shape factor = 0.9
  - $\lambda$  = X-ray wavelength, 1.5418 Å for CuK $\alpha$
  - $\theta$  = Observed peak angle, degree
  - $\beta$  = X-ray diffraction broadening, radian

The X-ray diffraction broadening ( $\beta$ ) is the pure width of a powder diffraction free of all broadening due to the experimental equipment. Standard  $\alpha$ -alumina is used to observe the instrumental broadening since its crystallite size is larger than 2000 Å. The X-ray diffraction broadening ( $\beta$ ) can be obtained by using Warren's formula.

From Warren's formula:

$$\begin{aligned} \beta^2 &= B_M^2 - B_S^2 \\ \beta &= \sqrt{B_M^2 - B_S^2} \end{aligned} \quad (\text{A.2})$$

- Where
- $B_M$  = The measured peak width in radians at half peak height.
  - $B_S$  = The corresponding width of a standard material.

**Example:** Calculation of the crystallite size of titanium dioxide

$$\begin{aligned} \text{The half-height width of 101 diffraction peak} &= 0.93125^\circ \\ &= 0.01625 \text{ radian} \end{aligned}$$

$$\text{The corresponding half-height width of peak of } \alpha\text{-alumina} = 0.002 \text{ radian}$$

$$\begin{aligned} \text{The pure width} &= \sqrt{B_M^2 + B_S^2} \\ &= \sqrt{0.01625^2 + 0.004^2} \\ &= 0.01612 \text{ radian} \end{aligned}$$

$$B = 0.01612 \text{ radian}$$

$$2\theta = 25.46^\circ$$

$$\theta = 12.73^\circ$$

$$\lambda = 1.5418 \text{ \AA}$$

$$\begin{aligned} \text{The crystallite size} &= \frac{0.9 \times 1.5418}{0.0157 \cos 12.73} = 100.5 \text{ \AA} \\ &= 10.05 \text{ nm} \end{aligned}$$

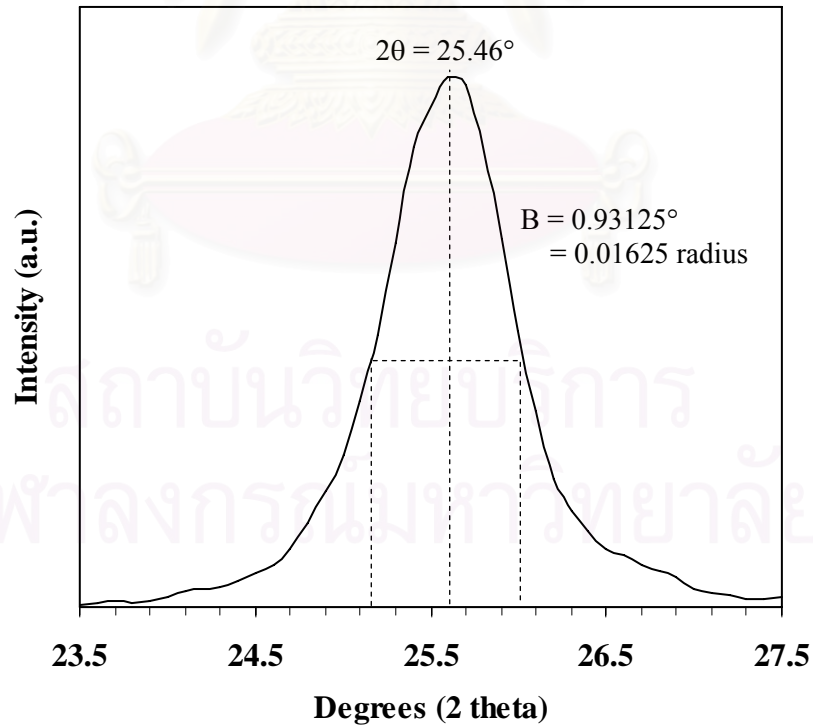


**Figure B.1** The 101 diffraction peak of titanium dioxide for calculation of the crystallite size



## APPENDIX C

### CALIBRATION CURVES

This appendix presented the calibration curve for calculation of products in photocatalytic reaction of water decomposition to hydrogen.

The thermal conductivity detector, gas chromatography Shimadzu model 8A was used to analyze the concentration of hydrogen by using Molecular sieve 5A column. The operating conditions for each instrument were described in the section 4.2.

Mole of hydrogen in y-axis and area reported by gas chromatography in x-axis are exhibited in the curves. The calibration curve of hydrogen is illustrated in the following Figure C.1.

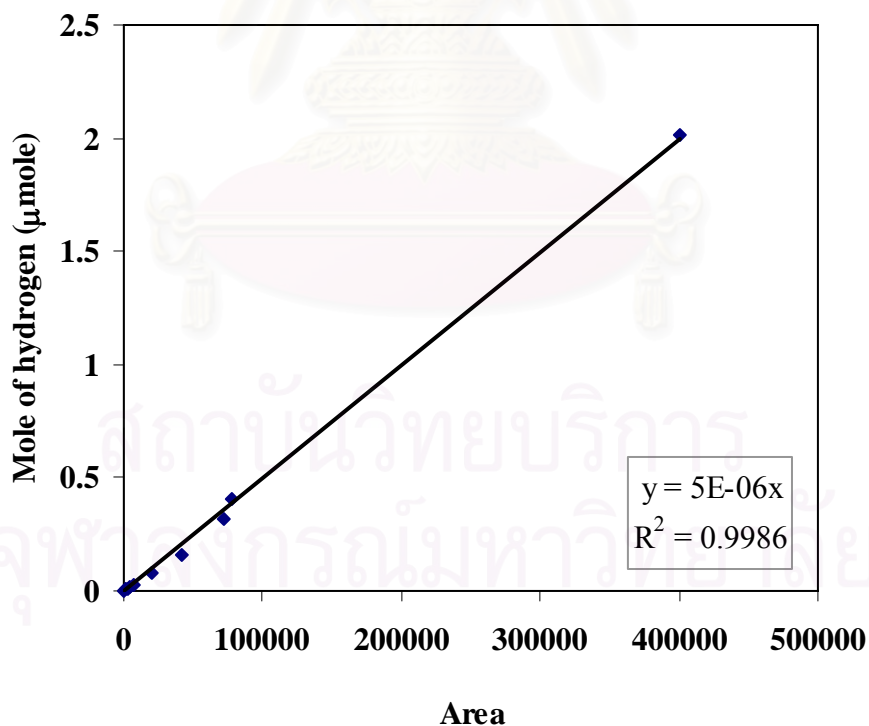


**Figure C.1** The calibration curve of hydrogen

**LIST OF PUBLICATION**

1. Eakachai Manatiwson, Akawat Sirisuk. “Bimetallic Doping of Titanium Dioxide for Use in Photocatalytic Splitting of Water”, Pure and Applied Chemistry International Conference 2008, Bangkok, Thailand, January 30- February 1, 2008.



สถาบันวิทยบริการ  
จุฬาลงกรณ์มหาวิทยาลัย

## VITA

Mr. Eakachai Manatiwson was born on December 8, 1983 in Saraburi, Thailand. He received the Bachelor Degree of Chemical Engineering from Faculty of Engineering, Burapha University in 2006. He continued his Master's study at Chulalongkorn University in June, 2006.



สถาบันวิทยบริการ  
จุฬาลงกรณ์มหาวิทยาลัย